A consistent framework for discrete integrations of soundproof and compressible PDEs of atmospheric dynamics

Piotr K. Smolarkiewicz, Christian Kühnlein, Nils P. Wedi

European Centre For Medium-Range Weather Forecasts, Reading, RG2 9AX, UK

Abstract

A numerical framework is developed for consistent integrations of soundproof and the fully compressible nonhydrostatic equations of motion for all-scale atmospheric flows; i.e., low Mach number, high-Reynolds number, rotating stratified flows under gravity. The reduced anelastic and pseudo-incompressible soundproof equations and the fully compressible Euler equations are combined into a common form of conservation laws for mass, momentum and entropy that facilitates the design of a sole principal algorithm for its integration, with minimal alterations for accommodating each special case. The development extends a proven numerical framework for integrating the soundproof equations. It relies on non-oscillatory forward-in-time transport methods, applied consistently to all dependent variables of the system at hand, and with buoyant and rotational modes of motion treated implicitly in the integration. When the fully compressible equations are solved, the framework admits congruent schemes with explicit or implicit representation of acoustic modes, so the former can provide a reference for the latter. The consistency of the framework minimises the numerical differences between the soundproof and compressible integrators, thus admitting conclusive comparisons between compressible and soundproof solutions, unobscured by algorithmic disparities. For the large-time-step implicit schemes, technical differences between the soundproof and compressible integrators reduce to the selection of either a prescribed or a numerically prognosed density, and extension of the generalised Poisson solver to a bespoke Helmholtz solver. The numerical advancements and merits of the approach are illustrated with canonical simulations of planetary baroclinic instability, an archetype of global weather, and the breaking of a deep stratospheric gravity waves, an example of nonhydrostatic mesoscale dynamics.

Key words: atmospheric models, non-oscillatory forward-in-time schemes, anelastic equations, compressible low Mach number flows, planetary weather, stratospheric gravity waves
PACS:

1 INTRODUCTION

The problems nowadays faced by numerical weather prediction (NWP) and climate models are intimately connected with the equations used and their numerical discretisation. Hydrostatic primitive equations (HPEs) have been successfully applied in weather and climate prediction for the past 30 years. However, with the rapid progress of high-performance computing, NWP models can already achieve globally spatial resolutions outside the domain of validity of HPEs because of their underlying hydrostatic balance assumption. While the capability to capture nonhydrostatic effects opens new avenues for all-scale simulations of atmospheric circulations [45,76], it also puts new demands on the mathematical/physical theories and on the numerical methods used. For example, the simulated vertical extent of the atmosphere is relatively thin compared to its horizontal extent, and vertically propagating sound waves admitted by the fully compressible Euler equations impose severe restrictions on the numerical algorithms used. HPEs are advantageous in this respect as they filter vertically propagating sound waves by virtue of the hydrostatic approximation, thus permitting large time steps in the numerical integration. Moreover, HPEs imply the separability of horizontal and vertical discretisation, thus facilitating the design of effective semi-implicit flow solvers. Both aspects have been central to the development and the success of weather and climate prediction.

The advance of massively parallel computing in the nineteen-nineties has stimulated broader interests of the atmospheric community in the development of nonhydrostatic models. With downscaling grid intervals, operational NWP codes naturally evolved towards extending their proven hydrostatic apparatus to the fully compressible Euler equations, from which the HPEs derive. Although no current NWP model runs globally at nonhydrostatic resolutions in operations, there is already substantial experience and the accumulated literature on integrating the all-scale Euler equations for weather and climate, and many operational models include nonhydrostatic options either for regional predictions or research [78,18,34,7,48,5,76]. Furthermore, as NWP models evolved by increasing the grid resolution, cloud-scale and mesoscale nonhydrostatic research models — originated more than three decades ago [71,11,24] — were extending their functionality by increasing the spatial domain [58,45,49,50,15]. The two paths of development were advancing their preferred integration methods for stiff PDEs — see [68] for an early review — with marked examples including semi-Lagrangian semi-implicit time integrators originated in NWP [78,18,34,7,48,76], and Eulerian split-explicit time stepping methods [45,49,5,50], a heritage of small-scale limited-area mod-

* Corresponding Author.
    Email address: `smolar@ecmwf.int` (Piotr K. Smolarkiewicz,).

els [71,24]. The assortment of schemes was further enhanced with various forms of spatial discretisation, including finite-differences [78,18,49,5], spectral transforms [78,7,76], finite-volumes [45,50], and more recently element-based Galerkin methods [15]. The technical literature devoted to the advancement of nonhydrostatic atmospheric models is extensive, and the references provided merely illustrate its diversity.

The imperative to drop the hydrostatic approximation with increasing resolution has opened a debate on the theoretical formulation optimal for NWP and climate models. The fully compressible Euler equations are universally valid for atmospheric motions across the range of scales from cloud micro-turbulence to planetary circulations. On the other hand, they admit acoustic modes — arguably of relatively little physical significance due to their low energy compared to other modes of motion — that provide serious computational drawbacks due to the large speed of sound in the stratified terrestrial atmosphere [28]. Notwithstanding, most efforts in NWP have been directed so far into solving the fully compressible equations, dismissing soundproof systems as unsuitable for modelling weather and climate based on scale or linear analysis; cf. [17] and references therein. Historically however, the majority of research in low Mach number flows under gravity, ranging from planetary atmospheres and oceans to mantle and solar convection, has relied on reduced soundproof equations that retain thermal aspects of compressibility but are free of acoustic modes. In particular, there is a body of literature attesting to the efficiency, accuracy, versatility and robustness of soundproof models permitting large time steps for a wide-ranging array of physical applications [64]. Accordingly, there is an interest to utilise the virtues of soundproof concepts in global nonhydrostatic NWP and climate models [20,1,4,29,8]. The current paper continues in this spirit, by combining the versatility and robustness of soundproof numerics with the compressible equations.

Herein, we document the development of a consistent numerical framework for conservative integrations of a suite of all-scale nonhydrostatic PDEs, including the anelastic [35,36], the pseudo-incompressible [19] and the fully compressible Euler equations of atmospheric dynamics. Philosophically akin to the recent work [8], but technically different, the present development augments an established multi-scale, multi-physics Eulerian/semi-Lagrangian, high-performance soundproof research model [42] with large-time-step semi-implicit integrators of the Euler equations. Moreover, a congruent acoustic scheme forms a special case of the framework and is used here for reference; yet, it is applicable to the study of gas dynamics at low and high Mach numbers in the context of atmospheric (and engineering) flows [63]. For simplicity and conciseness, the presentation is focused on the formulation of the conservative dynamical core; i.e., it is restricted to inviscid, adiabatic dry motions and only briefly alludes to the optional, congruent semi-Lagrangian integrators. For the numerical experimentation on large scales, an idealised problem of planetary

baroclinic instability [64] is adapted after [23]. For the simulation of non-hydrostatic scales of motion we select the non-Boussinesq amplification and breaking of stratospheric gravity waves, following calculations in [65]. These two problems epitomise the dynamics of planetary-scale Rossby waves and mesoscale gravity waves. Comparisons of the corresponding compressible and soundproof results verify and complement linear [17] and scale [27] analyses, corroborating the utility of the framework.

The paper is organised as follows. In the following section we first introduce the three sets of nonhydrostatic governing equations written in a physically intuitive Cartesian vector form, in abstraction from the model geometry and the coordinate frame adopted. Then, we combine the three sets into a single set recast in a form of the conservation laws consistent with the problem geometry and the unified solution procedure. The thrust of the paper is in section 3, where we build and document the common numerical algorithm for integrating the generalised set of the governing PDEs put forward in section 2. In section 4, we demonstrate the efficacy of this consistent numerical framework in the comparison of soundproof and compressible solutions to the two idealised flow problems relevant to weather and climate. Section 5 concludes the paper.

2 GOVERNING EQUATIONS

2.1 Anelastic Lipps-Hemler system

The most reduced analytically, and numerically the simplest, of the three nonhydrostatic systems considered in this paper is the Lipps-Hemler [35,36] anelastic set of equations, capable of simulating a broad range of atmospheric flows [27,64]. For the dry inviscid adiabatic dynamics addressed, these equations govern the evolution of momentum and entropy, constrained by the incompressible form of the mass continuity equation. In a rotating Cartesian reference frame, they can be compactly written as

$$\frac{d\mathbf{u}}{dt} = -\nabla\phi - \mathbf{g}\frac{\theta - \theta_b}{\theta_b} - \mathbf{f} \times \mathbf{u} \ , \tag{1}$$

$$\frac{d\theta}{dt} = 0 \ , \tag{2}$$

$$\nabla \cdot (\rho_b \mathbf{u}) = 0 \ . \tag{3}$$

Here, vector $\mathbf{u}$ denotes the flow velocity, and θ is the potential temperature — tantamount to specific entropy via $ds = c_p d\ln\theta$, with c_p denoting the specific heat at constant pressure. Notably, throughout this paper, "specific" refers to dependent variables that are expressed per unit of mass; e.g., the velocity can

4

be viewed as specific momentum. Furthermore, the differential operators of the total derivative d/dt and the nabla $\nabla = (\partial_x, \partial_y, \partial_z)$ have their generic meaning; so, $d/dt = \partial/\partial t + \mathbf{u} \cdot \nabla$. The Coriolis parameter is given as $\mathbf{f} \equiv 2\mathbf{\Omega}$, where $\mathbf{\Omega}$ denotes a constant angular velocity of the rotating reference frame. On the right-hand-side (rhs) of the momentum equation (1), $\phi \equiv c_p\theta_b(\pi - \pi_b)$ with $\pi \equiv (p/p_0)^{R_d/c_p}$ denoting the Exner-function of pressure, where R_d is the gas constant for dry air and p_0 is a constant reference pressure.[1] The subscript "$_b$" indicates the basic (reference) hydrostatically-balanced state of the anelastic asymptotic expansion. Here it assumes constant stratification $S = d\ln\theta_b/dz = N^2/g \geq 0$, with N and g denoting, respectively, the Brunt-Väisälä (buoyancy) frequency and the magnitude of the gravitational acceleration $\mathbf{g} = (0, 0, -g)$; altogether, this defines the background density stratification $\rho_b(z)$ [12].

To facilitate the presentation of numerical solution procedures, we introduce an auxiliary ambient state $(\mathbf{u}_e, \phi_e, \theta_e)$ assumed to be a known particular solution of the Lipps-Hemler system (1)-(3). By admitting alternative perturbation forms of the governing equations, the primary role of ambient states is to simplify the design of the initial and boundary conditions as well as to enhance the accuracy of calculations in finite-precision arithmetics. Generally, ambient states can be time-dependent; e.g., prescribing oceanic tidal motions [72]. In this paper, only stationary ambient states are considered, e.g., geostrophically and thermally balanced large-scale flows [58,62]. For illustration, consider subtracting

$$0 = -\nabla\phi_e - \mathbf{g}\frac{\theta_e - \theta_b}{\theta_b} - \mathbf{f} \times \mathbf{u}_e \tag{4}$$

from the momentum equation (1), and writing the entropy equation (2) in terms of perturbations about the geostrophic balance. This readily leads to the modified anelastic system

$$\frac{d\mathbf{u}}{dt} = -\nabla\phi' - \mathbf{g}\frac{\theta'}{\theta_b} - \mathbf{f} \times \mathbf{u}' , \tag{5}$$

$$\frac{d\theta'}{dt} = -\mathbf{u} \cdot \nabla\theta_e , \tag{6}$$

$$\nabla \cdot (\rho_b\mathbf{u}) = 0 , \tag{7}$$

in which primes appearing in the momentum and entropy equations denote perturbations with respect to the ambient state; so, $\phi' = c_p\theta_b(\pi - \pi_e)$, $\theta' = \theta - \theta_e$, and $\mathbf{u}' = \mathbf{u} - \mathbf{u}_e$.

Noteworthy, including the reference density under the gradient operator in the momentum equation (1), or (5), is a signature of the Lipps-Hemler system

---

[1] Note two useful relations: $\rho^{-1}\nabla p = c_p\theta\nabla\pi$; and $\pi = T/\theta$, where T indicates the temperature.

[36]. While it benefits the conditioning of the elliptic pressure equation [65], it also restricts baroclinic vorticity production to thermally driven circulations in vertical planes [62].

2.2 Pseudo-incompressible Durran system

Analytically more general, yet more challenging numerically, is the pseudo-incompressible soundproof system of Durran [19]. Compared to the anelastic equations, the pseudo-incompressible system is a lesser abbreviation of the compressible Euler equations, thus potentially capable to simulate a broader range of atmospheric flows [17,27,3,64]. In analogous notation to the Lipps-Hemler system (5)-(7), the pseudo-incompressible equations can be compactly written as

$$\frac{d\mathbf{u}}{dt} = -c_p\theta\nabla\pi' - \mathbf{g}\frac{\theta'}{\theta_e} - \mathbf{f} \times \left(\mathbf{u} - \frac{\theta}{\theta_e}\mathbf{u}_e\right) \ , \tag{8}$$

$$\frac{d\theta'}{dt} = -\mathbf{u} \cdot \nabla\theta_e \ , \tag{9}$$

$$\nabla \cdot \left(\rho_b\frac{\theta_b}{\theta_0}\mathbf{u}\right) = 0 \ , \tag{10}$$

where θ_0 marks a constant reference value of θ, and where we assume the same constant-stability basic-state profile (denoted by subscript $_b$) as in the Lipps-Hemler system. This does not necessarily imply the same balanced ambient state. In particular, a large-scale geostrophically-balanced thermal wind will be different for the two systems, because it derives as a compatibility condition from the governing equations. The geostrophic balance assumed in (8) satisfies

$$0 = -c_p\theta_e\nabla(\pi_e - \pi_b) - \mathbf{g}\frac{\theta_e - \theta_b}{\theta_b} - \mathbf{f} \times \mathbf{u}_e \ , \tag{11}$$

as opposed to (4).

Noteworthy, in contrast to the Lipps-Hemler equations, the Durran system retains the full, unapproximated form of the (specific) momentum equation, with the complete baroclinic vorticity source. As far as the solutions are sought for $\mathbf{u}$ and θ, the definition of the (diagnostic) pressure variable is flexible, because pressure in soundproof models adapts to the explicit part of the elliptic boundary value problem (implied by the mass continuity) and boundary conditions. Consequently, the pressure gradient force in (8) has two contributions given as

$$-c_p\theta\nabla\pi' = -\nabla\phi' + \phi'\nabla\ln\theta \ , \tag{12}$$

where the first term on the rhs is analogous to the Lipps-Hemler pressure gradient. This, together with a more slowly decaying density of the pseudo-incompressible system, $\rho_b(\theta_b/\theta_0)$, hints at the difference between the pseudo-incompressible and the anelastic system, expected to amplify with increasing stratification or increasing spatial scales of the simulated phenomena. Furthermore, in the small-scale limit where basic profiles ρ_b, θ_b converge to constant reference values ρ_0, θ_0, the pseudo-incompressible and anelastic systems reduce, respectively, to the incompressible Euler and Boussinesq equations [17,62,26,27,3].

2.3 Compressible Euler equations

The compressible Euler equations that encompass the reduced soundproof systems can be written in a variety of analytically-equivalent forms. Because the goal of this paper is to present consistent conservative integrators of all three systems, the compressible equations are written in a particular form emphasising the similarity of the three systems: [2]

$$\frac{d\mathbf{u}}{dt} = -c_p\theta\nabla\pi' - \mathbf{g}\frac{\theta'}{\theta_e} - \mathbf{f} \times \left(\mathbf{u} - \frac{\theta}{\theta_e}\mathbf{u}_e\right) \ , \tag{13}$$

$$\frac{d\theta'}{dt} = -\mathbf{u} \cdot \nabla\theta_e \ , \tag{14}$$

$$\frac{d\rho}{dt} = -\rho\nabla \cdot \mathbf{u} \ , \tag{15}$$

$$\pi = \left(\frac{R_d}{p_0}\rho\theta\right)^{R_d/c_v} \ , \tag{16}$$

where specific heat at constant volume is $c_v = c_p - R_d$. Here, the balanced ambient state coincides with that of the pseudo-incompressible system, because the evolution of specific momentum is governed by analogous equations in both systems; cf. (8) and (13).

Noteworthy, the Lipps-Hemler and the Durran equations, (5)-(7) and (8)-(10), do not necessitate the provision of constitutive laws for their solution, because their respective pressure perturbations are determined from the elliptic equations that follow from constraining the velocity solutions to satisfy mass continuity, i.e. (7) and (10). In other words, their constitutive laws were analytically accounted for while deriving the reduced equations, and afterwards are not required unless there is a need to provide, say, temperature perturbations for moist thermodynamics [31]. This is not the case with fully

---

[2] In contrast to the soundproof systems, the Euler equations are free of any linearisations that discard perturbational terms as negligibly small.

compressible equations where the ideal gas law in (16) explicitly relates the thermodynamic pressure perturbations to the distribution of temperature and mass in the fluid.

2.4   A combined symbolic system

It is practical to view the three PDE systems of sections 2.1-2.3 as special cases of a single generalised equation set, regardless of the profound physical and mathematical implications of the soundproof mass continuity equations (7) and (10) compared to the fully compressible case (15). The generalised system can be compactly written as

$$\frac{d\mathbf{u}}{dt} = -\Theta\nabla\varphi - \mathbf{g}\Upsilon_B\frac{\theta'}{\theta_b} - \mathbf{f} \times (\mathbf{u} - \Upsilon_C\mathbf{u}_e) \; , \tag{17}$$

$$\frac{d\theta'}{dt} = -\mathbf{u} \cdot \nabla\theta_e \; , \tag{18}$$

$$\frac{d\varrho}{dt} = -\varrho\nabla \cdot \mathbf{u} \; . \tag{19}$$

Here, the generalised density and pressure variables ϱ and φ are defined, respectively, for the [anelastic, pseudo-incompressible, compressible] PDE sets as

$$\varrho := \left[\rho_b(z), \; \rho_b\frac{\theta_b(z)}{\theta_0}, \; \rho(\mathbf{x},t)\right] \; , \tag{20}$$

$$\varphi := [c_p\theta_b\pi', \; c_p\theta_0\pi', \; c_p\theta_0\pi'] \; , \tag{21}$$

together with corresponding dimensionless coefficients

$$\Theta := \left[1, \; \frac{\theta(\mathbf{x},t)}{\theta_0}, \; \frac{\theta(\mathbf{x},t)}{\theta_0}\right] \; , \tag{22}$$

$$\Upsilon_B := \left[1, \; \frac{\theta_b(z)}{\theta_e(\mathbf{x})}, \; \frac{\theta_b(z)}{\theta_e(\mathbf{x})}\right] \; , \tag{23}$$

$$\Upsilon_C := \left[1, \; \frac{\theta(\mathbf{x},t)}{\theta_e(\mathbf{x})}, \; \frac{\theta(\mathbf{x},t))}{\theta_e(\mathbf{x})}\right] \; . \tag{24}$$

The generalised system (17)-(19) takes a form of compressible equations, which can be misleading if taken out of context. Clearly, its interpretation depends on the definition of the generalised density used in (19), as a prescribed problem parameter for the anelastic and pseudo-incompressible systems (20), or as a

8

dependent prognostic variable with the associated constitutive law

$$\varphi = c_p \theta_0 \left[\left(\frac{R_d}{p_0} \varrho \theta \right)^{R_d/c_v} - \pi_e \right] . \tag{25}$$

2.5 Conservative formulation

The set of PDEs (17)-(19) can be further manipulated to generate abstract forms useful for designing flux-form numerical integrators. For example, combining $\varrho \cdot$(17) with $\mathbf{u} \cdot$(19), and $\varrho \cdot$(18) with $\theta' \cdot$(19), and combining the rhs of (19) with the total derivative $d\varrho/dt$ on the left-hand-side (lhs), leads to the set of conservation laws

$$\frac{\partial \varrho \mathbf{u}}{\partial t} + \nabla \cdot (\varrho \mathbf{u} \otimes \mathbf{u}) = \varrho \boldsymbol{R}^{\mathbf{u}} , \tag{26}$$

$$\frac{\partial \varrho \theta'}{\partial t} + \nabla \cdot (\varrho \mathbf{u} \theta') = \varrho R^\theta , \tag{27}$$

$$\frac{\partial \varrho}{\partial t} + \nabla \cdot (\varrho \mathbf{u}) = 0 , \tag{28}$$

wherein $\boldsymbol{R}^{\mathbf{u}}$ and R^θ symbolise right-hand-sides of (17) and (18), respectively, and $\otimes$ denotes the tensor product. The prognostic momentum (17) and entropy (18) equations can be viewed as the generic Lagrangian form

$$\frac{d\psi}{dt} = R , \tag{29}$$

whereas (26) and (27) can be viewed as the generic conservation law

$$\frac{\partial \varrho \psi}{\partial t} + \nabla \cdot (\varrho \mathbf{u} \psi) = \varrho R , \tag{30}$$

with ψ symbolising the three components of the velocity vector and potential temperature perturbation, while R denotes the associated right-hand-sides.

2.6 Generalised coordinate description

In NWP and climate models, continuous mappings using general curvilinear coordinates are favoured, simplifying theories and models by reflecting natural material structure of atmosphere and oceans [73]. All developments in this paper are implemented in the established soundproof model EULAG (Eulerian/semi-Lagrangian fluid solver, [42]), formulated in the generalised time-dependent curvilinear coordinates to enable dynamic mesh adaptivity; see [41,73,30,66] and the references therein. The current developments use the

9

stationary subset of this capability, by assuming zero mesh velocity. Consequently all relevant formulae in section 3.2 are valid for spatial coordinates independent of time. Despite that, further discussions allude to the generalised time-dependent coordinate description, because the advancements presented in this paper were inspired by the generalised forms and geometric considerations in the recent work [30] on soundproof modelling of atmospheric flows with adaptive moving meshes. The results of [30] indicate that soundproof models in time-dependent coordinates have much in common with compressible flow solvers. Thus, combining the mathematical/numerical apparatus of soundproof equations cast in time-dependent coordinates with the numerics of akin integrators for transonic and supersonic gas dynamics in stationary coordinates [63], generalises into the consistent numerical framework for soundproof and compressible equations presented in section 3.2.

In this generalised time-dependent curvilinear coordinate description, (28) naturally takes the compressible form,

$$\frac{\partial \mathcal{G} \varrho}{\partial t} + \nabla \cdot (\mathcal{G} \varrho \mathbf{v}) = 0 \ , \tag{31}$$

regardless of the definition of ϱ in (20). In (31), $(\mathbf{x}, t)$ refers already to the coordinates of the generalised time-dependent frame, and $\mathcal{G}(\mathbf{x}, t)$ denotes the Jacobian.[3] As in section 2, $\nabla \cdot ..$ denotes the scalar product of spatial partial derivatives with a vector, so $d/dt = \partial/\partial t + \mathbf{v} \cdot \nabla$, with the velocity $\mathbf{v} = \dot{\mathbf{x}}$ not necessarily equal to $\mathbf{u}$. Notably, the compressible form of (31) can result from either variability of the coordinates in time, compressibility per se, or both.[4] The corresponding extension of (26) and (27) to a common symbolic form for a specific variable ψ is

$$\frac{\partial \mathcal{G} \varrho \psi}{\partial t} + \nabla \cdot (\mathcal{G} \varrho \mathbf{v} \psi) = \mathcal{G} \varrho R \ , \tag{32}$$

with some modifications of the right-hand-sides.[5] Importantly, the generalised mass continuity equation (31) is a special case of (32), with predetermined $\psi \equiv 1$ and $R \equiv 0$ for all $(\mathbf{x}, t)$ and equation sets. This makes the mass continuity distinct from conservation laws for specific dependent variables ψ, and

---

[3] Mathematical details of differential geometry are unimportant for this motivational argument; for completeness, however, we recall that $\mathcal{G}^2$ is the determinant of the metric tensor that defines the fundamental metric in a space of interest where the problem is solved [41].

[4] Vice versa, an incompressible form of the continuity equation may result in a compressible system with suitable variability of coordinates in time; e.g. $\mathcal{G} \varrho = \text{const.}$, as for mass-based coordinates commonly used in atmospheric models [32].

[5] For instance, $\nabla \varphi$ in the momentum equation is replaced with the product of a coefficient matrix and the vector of partial derivatives, $\widetilde{\mathbf{G}} \nabla \varphi$, and $\mathbf{u}$ on the rhs of the perturbation form of the θ equation is replaced by $\widetilde{\mathbf{G}}^T \mathbf{u} = \mathbf{v} - \mathbf{v}^g$ where $\mathbf{v}^g$ denotes the mesh velocity, set to zero in sections 3.2.2 and 3.2.3.

its primordial role for the design of the consistent integration framework of soundproof and compressible systems of PDEs is shown in the next section.

3   INTEGRATION SCHEMES

3.1   Non-oscillatory forward-in-time differencing for fluids

The term "non-oscillatory forward-in-time" (hereafter NFT) labels a class of second-order-accurate two-time-level algorithms built on nonlinear advection schemes that suppress/reduce/control numerical oscillations characteristic of higher-order linear schemes. Forward-in-time techniques are standard in computational meteorology, particularly in the context of semi-Lagrangian schemes [78,18,7,76,77]. Their virtues, compared to second-order-accurate centred-in-time three-time-level methods [11,34], include lower dispersion errors and a lower storage requirement. On the other hand, whenever the intermediate time-centred field values are required — e.g., for nonlinear non-dissipative forces [18,66] — FT schemes lead to implicit problems often necessitating iterative solutions [18,7,66]. Here we are primarily concerned with flux-form NFT schemes, the conservativity of which is important for simulation of atmospheric acoustics [63], chemical tracers [33,77], climate studies [1,2,77] and accurate representation of slow oscillations in planetary and stellar atmospheres [74,21]. Last but not least, the addressed flux-form NFT schemes, naturally lend themselves to imposing flux boundary conditions and generalisation to congruent finite-volume methods on unstructured meshes [60,63,70,65,67].

An instructive archetype problem to consider is the generalised transport equation for an arbitrary scalar variable Ψ,

$$\frac{\partial G\Psi}{\partial t} + \nabla \cdot (\mathbf{V}\Psi) = G\mathcal{R} , \tag{33}$$

where the vector field $\mathbf{V}$ and scalar coefficients G and $\mathcal{R}$ are assumed to be known functions of time and space. Although (33) is reminiscent of (31) and (32), it matches neither of them exactly; we shall return to this point shortly. A forward-in-time (FT) discretisation of (33) with respect to Ψ is assumed as

$$\frac{G^{n+1}\Psi^{n+1} - G^n\Psi^n}{\delta t} + \nabla \cdot (\mathbf{V}^{n+1/2}\Psi^n) = \left(G\mathcal{R}\right)^{n+1/2} , \tag{34}$$

where n and $n+1$ index the levels of a uniform temporal grid $t^{n+1} = t^n + \delta t$, and $n+1/2$ refers to $\mathcal{O}(\delta t^2)$ estimates at an intermediate time level. Standard truncation-error analysis — i.e., expanding all terms in the second-order Taylor series about t^n and representing second-order temporal partial derivatives

11

in terms of the spatial derivatives based on the structure of the governing equation (33) [57,61] — leads to the modified equation that is approximated by (34) to $\mathcal{O}(\delta t^2)$:

$$\frac{\partial G\Psi}{\partial t} + \nabla \cdot (\mathbf{V}\Psi) = G\mathcal{R}$$
$$- \nabla \cdot \left[\frac{\delta t}{2} G^{-1} \mathbf{V}(\mathbf{V} \cdot \nabla\Psi) + \frac{\delta t}{2} G^{-1} \left(\frac{\partial G}{\partial t} + \nabla \cdot \mathbf{V} \right) \mathbf{V}\Psi \right] \qquad (35)$$
$$+ \nabla \cdot \left(\frac{\delta t}{2} \mathbf{V}\mathcal{R} \right) + \mathcal{O}(\delta t^2) \ .$$

The modified equation (35) reveals the functional form of the $\mathcal{O}(\delta t)$ error due to the uncentred-in-time differencing of Ψ in (34).

To derive a fully second-order-accurate FT algorithm, (34) is supplied on the rhs with explicit, at least first-order accurate, discrete representations of the negative of the error, thus compensating the error to at least $\mathcal{O}(\delta t^2)$. The first divergence expression on the rhs of (35) is intricate but does not depend on $\mathcal{R}$. Its compensation is within the realm of multidimensional FT flux-form advection schemes such the "multidimensional positive definite advection transport algorithm" (MPDATA) [51,30] used throughout this work for the NFT advection. [6] The second divergence expression on the rhs of (35) is compact, does not depend on Ψ, and it couples the advection and forcing. Many implementations of FT algorithms treat advection separately from the forcings, in analogy to centred-in-time-and-space methods. However, leaving this error uncompensated amplifies oscillations and can lead to instability. Its compensation is technically simple and merely requires a proper implementation of the rhs forcing [56]. Consider a second-order accurate NFT advection scheme for the homogeneous case ($\mathcal{R} \equiv 0$) of (33):

$$\Psi_{\mathbf{i}}^{n+1} = \frac{G_{\mathbf{i}}^n}{G_{\mathbf{i}}^{n+1}} \left(\Psi_{\mathbf{i}}^n - \frac{\delta t}{G_{\mathbf{i}}^n} \nabla \cdot \overline{(\mathbf{V}\Psi)}^{n+1/2} \right) + \mathcal{O}(\delta t^3) \qquad (36)$$
$$\equiv \mathcal{A}_{\mathbf{i}} \left(\Psi^n, \mathbf{V}^{n+1/2}, G^n, G^{n+1} \right) + \mathcal{O}(\delta t^3) \ ,$$

where a vector index $\mathbf{i} = (i_1, i_2, i_3)$ marks the point $\mathbf{x_i}$ of a co-located grid. The expression on the rhs of (36) encapsulates the FT Taylor-series derivation procedure by expressing its final product as an effectively centred-in-time integral of the homogeneous (33), symbolised with an overline atop the advective flux. The identity that follows in the second line of (36) defines an advection transport operator in terms of its entries, with details of $\mathcal{A}$ provided in

---

[6] The MPDATA has been developed over three decades and is widely documented in the literature; see [57,61] for reviews. It is briefly summarised in the appendix A.

the appendix A. Given (36), a second-order-accurate solution to (33) can be generated as

$$\Psi_{\mathbf{i}}^{n+1} = \mathcal{A}_{\mathbf{i}}\left(\widetilde{\Psi}^n, \mathbf{V}^{n+1/2}, G^n, G^{n+1}\right) + 0.5\delta t \mathcal{R}_{\mathbf{i}}^{n+1} , \tag{37}$$

where

$$\widetilde{\Psi}^n \equiv \Psi^n + 0.5\delta t \mathcal{R}^n . \tag{38}$$

Transporting the auxiliary field $\widetilde{\Psi}^n$ (as opposed to Ψ^n) — i.e. using in (34) $(G\mathcal{R})^{n+1/2} = 0.5(G\mathcal{R})^n + 0.5(G\mathcal{R})^{n+1} + \mathcal{O}(\delta t^2)$, and incorporating $0.5(G\mathcal{R})^n$ in the advective operator $\mathcal{A}$ — compensates the third term on the rhs of (35) [56].

Depending on the definitions of G, Ψ, $\mathbf{V}$ and $\mathcal{R}$, the outlined archetype PDE (33) and its NFT integrator (37) solve problems such as (32) formulated in terms of specific dependent variables (expressed per unit of mass), or solve problems formulated in terms of dependent variables expressed per unit of volume, the simplest example of which is (31). In the former case, typical of the soundproof models, the density ϱ is absorbed in $G \equiv \mathcal{G}\varrho$, whereas $\Psi \equiv \psi$ and $\mathcal{R} \equiv R$. In the latter case, typical of gas dynamics, the density is absorbed in $\Psi \equiv \varrho\psi$, whereas $G \equiv \mathcal{G}$ and $\mathcal{R} \equiv \varrho R$. In both cases $\mathbf{V} \equiv G\mathbf{v}$, upon which $\mathbf{V} \equiv \mathcal{G}\varrho\mathbf{v}$ or $\mathbf{V} \equiv \mathcal{G}\mathbf{v}$, respectively, for Ψ representing a specific or a density type variable. This duality of the interpretation benefits the efficacy of FT solvers, clearly by admitting computational research across a broad range of scales and physical scenarios [72,42,63,70,21,66].

Notwithstanding the universality of the NFT integrators in (37), from the perspective of designing large-time-step semi-implicit compressible solvers, the soundproof MPDATA based integrators offer substantial advantages. For example, they automatically cancel first-order truncation errors depending on the flow divergence, regardless of the complexity of the curvilinear framework. Furthermore, in stationary frameworks, the soundproof integrators naturally assure — given a sufficiently accurate solution of the elliptic pressure equation [66] — that flux-form advection does not generate spurious tendencies of specific variables wherever these variables are locally constant [30]. Also, limiting the transportive momenta $\mathcal{G}\varrho\mathbf{v}$ [53]— as opposed to limiting the transportive velocities $\mathcal{G}\mathbf{v}$ in compressible models [46,69,63] — controls extrema of specific variables consistently with their (physically meaningful) Lagrangian evolution [53,46,30]. The latter two advantages are important for simulating atmospheric flows, where actual perturbations of potential temperature, density and pressure often represent a tiny fraction of the background values. The most consequential however, is that the soundproof NFT integrator (37) naturally lends itself to implicit representations of the rhs forcing [42].[7] Taking

---

[7] This is not necessarily the case with the compressible integrators in the spirit of

into account all pros and cons, we chose to extend large-time-step soundproof integrators to weakly compressible atmospheric flows, rather than extending the capabilities of gas dynamics integrators to large-time-step simulations of low Mach number flows.

3.2   Consistent NFT framework

The remainder of this section shows how to extend the soundproof NFT integrators to the fully compressible equations, and that this reduces to two key modifications: (i) utilise the compressible mass continuity equation in (31) together with its naturally associated compressible integrator in (36) to prognose the density, while concomitantly defining the transportive momenta for all specific variables; and   (ii) extend the generalised Poisson solver of the soundproof models to Helmholtz problems arising due to the constitutive law (25), together with the numerical formulation of the soundproof integrator in (37). The modification (i) is important for minimising numerical departures between the soundproof and the compressible models, and it suffices for compressible integrations with acoustic time steps; i.e., limited by the CFL condition based on the speed of sound. The modification (ii) is essential to enable integrating compressible equations with larger time steps. The two modifications together lead to a class of conservative compressible NFT schemes with the mass continuity equation integrated in the spirit of gas dynamics [63], but with the entropy and momentum equations integrated in the spirit of soundproof equations arising in time-dependent geometry [30]. In the following paragraph, we apply (i) in the context of the compressible Euler equations under gravity and rotation. The resulting algorithm is explicit with respect to acoustic modes (hereafter an "acoustic scheme"), yet implicit with respect to buoyant and rotational modes. This unusual scheme is a derivative of the proven NFT integrator for the soundproof equations [42] and prepares the grounds for large-time-step semi-implicit integrators. Section 3.2.3 discusses (ii) and the incorporation into the acoustic scheme of bespoke Helmholtz solvers.

3.2.1   Transportive momenta for specific variables in compressible flows

Advecting specific variables with mass fluxes has a long tradition in computational fluid dynamics. In flux-form anelastic models, it arises naturally [11,52] as a byproduct of an exact-projection formulation of the elliptic pressure equation that follows the anelastic mass-continuity constraint. In elastic systems, it assures compatibility of finite-volume advection with Lagrangian transport

gas dynamics [63], for which the inherent nonlinearity of the conservation laws may lead to complex nonlinear elliptic problems.

14

of the specific variables [33,10,26] and facilitates extensions of compressible schemes to the soundproof regime [25,47,26]. Here it facilitates the extension of soundproof schemes to the compressible regime, while still assuring the compatibility of finite-volume advection with Lagrangian transport.

Standardly, the transportive momenta and advective velocities $\mathbf{V}^{n+1/2}$ that enter (36) and (37) are evaluated by linear extrapolation from $n-1$ and n time levels, which requires storing an additional vector field. This is preferred for soundproof models, as it assures that the advective momenta satisfy mass continuity by design. Alternatively, solving the full equation of motion to the first order [57] circumvents the necessity of storing an extra vector field, and benefits the stability of explicit solvers for elastic systems [56]. In calculations reported in section 4, all soundproof integrations use the former. In accord with the previous discussion (in the ending of section 3.1 and the opening of section 3.2), here we consider another alternative, bespoke for the mixed problem of the fully compressible case. Firstly, the prognostic mass continuity equation (31) is evaluated with $\mathbf{V}^{n+1/2} = (\mathcal{G}\mathbf{v})^{n+1/2}$ in (36) — for large-time-step calculations the linear extrapolation is used, whereas for acoustic runs the first order nonlinear predictor is employed. Secondly, all remaining PDEs are viewed as (32) in terms of specific variables ψ, and employ the soundproof variant of (37) with transportive momenta $\mathbf{V}^{n+1/2} = \overline{(\mathcal{G}\varrho\mathbf{v})}^{n+1/2}$ defined as cumulative (over MPDATA iterations) advective mass fluxes, evaluated in (36) while transporting ϱ; see appendix B for details.

3.2.2 A semi-implicit acoustic scheme

As a preamble to semi-implicit schemes for large-time-step integrations of the compressible Euler equations, consider a semi-implicit algorithm for integrating the compressible equations with explicit representation of acoustic modes in (17)-(19), cast in stationary curvilinear coordinates (e.g., to accommodate surface orography):

$$\frac{\partial \mathcal{G}\varrho}{\partial t} + \nabla \cdot (\mathcal{G}\varrho\mathbf{v}) = 0 \ , \tag{39}$$

$$\frac{\partial \mathcal{G}\varrho\theta'}{\partial t} + \nabla \cdot (\mathcal{G}\varrho\theta'\mathbf{v}) = -\mathcal{G}\varrho\widetilde{\mathbf{G}}^T\mathbf{u} \cdot \nabla\theta_e \ ,$$

$$\frac{\partial \mathcal{G}\varrho\mathbf{u}}{\partial t} + \nabla \cdot (\mathcal{G}\varrho\mathbf{v} \otimes \mathbf{u}) =$$

$$-\mathcal{G}\varrho\left(\Theta\widetilde{\mathbf{G}}\nabla\varphi + \mathbf{g}\Upsilon_B\frac{\theta'}{\theta_b} + \mathbf{f} \times (\mathbf{u} - \Upsilon_C\mathbf{u}_e) - \mathcal{M}'(\mathbf{u}, \mathbf{u}, \Upsilon_C)\right) \ .$$

Here, the notation combines those of sections 2.4 and 2.6, while incorporating further symbolism of Riemannian geometry with $\mathbf{v} = \widetilde{\mathbf{G}}^T\mathbf{u}$ and $\widetilde{\mathbf{G}}$ denoting the matrix of known metric coefficients [41,66]. The term $\mathcal{M}'(\mathbf{u}, \mathbf{u}, \Upsilon_C) =$

$\mathcal{M}(\mathbf{u}, \mathbf{u}) - \mathcal{M}(\mathbf{u}_e, \mathbf{u}_e)$ symbolises metric forcings in the spherical domain; see Appendix A of [66].

In the system (39), only the mass continuity equation is homogeneous, whereas the entropy and momentum equations have non-vanishing right-hand-sides, dependent on the prognosed model variables. In consequence, the entire model algorithm reduces to two conceptually distinct steps. In the first step the density becomes updated, while constructing the transportive momenta required for the subsequent update of specific variables of potential temperature and velocity components:

$$\varrho_{\mathbf{i}}^{n+1} = \mathcal{A}_{\mathbf{i}}\left(\varrho^n, (\mathcal{G}\mathbf{v})^{n+1/2}, \mathcal{G}, \mathcal{G}\right) \quad \Longrightarrow \quad \mathbf{V}^{n+1/2} = \overline{(\mathcal{G}\varrho\mathbf{v})}^{n+1/2} . \tag{40}$$

In the second step, to account for the nonlinearity of the pressure gradient force and the metric forces on the rhs of the momentum equations, the template algorithm (37) is executed iteratively, lagging nonlinear terms behind:

$$\theta'|_{\mathbf{i}}^{\nu} = \widehat{\theta}_{\mathbf{i}}' - 0.5\delta t \left(\widetilde{\mathbf{G}}^T \mathbf{u}^\nu \cdot \nabla \theta_e\right)_{\mathbf{i}} \tag{41}$$

$$\mathbf{u}_{\mathbf{i}}^\nu = \widehat{\mathbf{u}}_{\mathbf{i}} - 0.5\delta t \left(\Theta^{\nu-1}\widetilde{\mathbf{G}}\nabla\varphi^\nu + \mathbf{g}\Upsilon_B \frac{\theta'^\nu}{\theta_b}\right)_{\mathbf{i}}$$

$$- 0.5\delta t \left(\mathbf{f} \times (\mathbf{u}^\nu - \Upsilon_C^{\nu-1}\mathbf{u}_e) - \mathcal{M}'(\mathbf{u}, \mathbf{u}, \Upsilon_C)^{\nu-1}\right)_{\mathbf{i}} .$$

Here, $\widehat{\theta}_{\mathbf{i}}'$ and $\widehat{\mathbf{u}}_{\mathbf{i}}$ are the shorthands for the transport operator $\mathcal{A}$ applied to $\widetilde{\theta}'$ and $\widetilde{\mathbf{u}}$ in (37)-(38), given as

$$\widehat{\theta}_{\mathbf{i}}' = \mathcal{A}_{\mathbf{i}}\left(\widetilde{\theta}', \mathbf{V}^{n+1/2}, \varrho^{*n}, \varrho^{*n+1}\right) , \tag{42}$$

$$\widehat{\mathbf{u}}_{\mathbf{i}} = \mathcal{A}_{\mathbf{i}}\left(\widetilde{\mathbf{u}}, \mathbf{V}^{n+1/2}, \varrho^{*n}, \varrho^{*n+1}\right) ,$$

with $\mathbf{V}^{n+1/2}$ provided by (40), and the effective densities ϱ^{*n} and ϱ^{*n+1} defined, respectively, as $\varrho^{*n} := \mathcal{G}\varrho^n$ and $\varrho^{*n+1} := \mathcal{G}\varrho^{n+1}$. Furthermore,

$$\varphi_{\mathbf{i}}^\nu = c_p \theta_0 \left[\left(\frac{R_d}{p_0}\varrho^{n+1}\theta^{\nu-1}\right)^{R_d/c_v} - \pi_e\right]_{\mathbf{i}} , \tag{43}$$

$$\theta_{\mathbf{i}}^\nu = \left(\widehat{\theta}' - 0.5\delta t\widetilde{\mathbf{G}}^T\mathbf{u}^\nu \cdot \nabla\theta_e + \theta_e\right)_{\mathbf{i}} . \tag{44}$$

Throughout (41)-(44), the index $\nu = 1, .., N_\nu$ numbers the iterations, with the first guess $\theta_{\mathbf{i}}^0 = \widehat{\theta}_{\mathbf{i}}$ generated by advecting full θ,

$$\theta_{\mathbf{i}}^0 = \mathcal{A}_{\mathbf{i}}\left(\theta^n, \mathbf{V}^{n+1/2}, \varrho^{*n}, \varrho^{*n+1}\right) \tag{45}$$

16

and $\mathbf{u_i^0}$ obtained by solving the advective form of the momentum equation to the first order [56]. With this design, the solution is fully second order accurate even for $N_\nu = 1$, and $N_\nu = 2$ gives already close approximation to the trapezoidal integral [63].

The scheme outlined in (41)-(44) contains fully implicit trapezoidal integrals of buoyancy and Coriolis terms; whereas pressure perturbations (viz. acoustic modes), metric forcings, and coefficients depending on full potential temperature are integrated explicitly. To derive the closed-form expression for the velocity update, we substitute the potential temperature perturbation in the buoyancy term of the momentum equation with the rhs of the entropy scheme and gather all terms depending on $\mathbf{u}^\nu$ on the lhs of the momentum scheme, while dropping the spatial grid index $\mathbf{i}$ everywhere, as all dependent variables, coefficients and terms are co-located in (41)-(44). This results in

$$\mathbf{u}^\nu + 0.5\delta t \mathbf{f} \times \mathbf{u}^\nu - (0.5\delta t)^2 \mathbf{g}\Upsilon_B \frac{1}{\theta_b}\widetilde{\mathbf{G}}^T \mathbf{u}^\nu \cdot \nabla\theta_e = \tag{46}$$

$$\widehat{\mathbf{u}} - 0.5\delta t\left(\mathbf{g}\Upsilon_B\frac{\widehat{\theta'}}{\theta_b} - \mathbf{f} \times \Upsilon_C^{\nu-1}\mathbf{u}_e - \mathcal{M}'(\mathbf{u},\mathbf{u},\Upsilon_C)^{\nu-1}\right)$$

$$-0.5\delta t\Theta^{\nu-1}\widetilde{\mathbf{G}}\nabla\varphi^\nu \quad \equiv \quad \widehat{\widehat{\mathbf{u}}} - 0.5\delta t\Theta^{\nu-1}\widetilde{\mathbf{G}}\nabla\varphi^\nu \ ,$$

which symbolises a system of three linear algebraic equations with three unknown components of the velocity vector $\mathbf{u}^\nu$ at each point of the co-located grid. Viewing the lhs of (46) as a linear operator acting on the velocity vector, $\mathbf{L}\mathbf{u}^\nu$, the closed-form expression for the velocity update may be symbolised as

$$\mathbf{u}^\nu = \breve{\mathbf{u}} - \mathbf{C}\nabla\varphi^\nu \ , \tag{47}$$

where $\breve{\mathbf{u}} = \mathbf{L}^{-1}\widehat{\widehat{\mathbf{u}}}$ and $\mathbf{C} = \mathbf{L}^{-1}0.5\delta t\Theta^{\nu-1}\widetilde{\mathbf{G}}$ denotes a 3×3 matrix of known coefficients; cf. [41] and [65,67] for expanded expressions in tensorial and explicit component notations. In each iteration ν the velocity update in (47) uses the thermodynamic pressure in (43), and the total potential temperature (required in the coefficients Θ and Υ_C) gets updated according to (44). The potential temperature perturbation θ' is updated according to (41), upon completion of the velocity update for $\nu = N_\nu$.

The acoustic scheme given above originated from an adaptation of the sound-proof pseudo-incompressible algorithm [62,65], as an extension of the anelastic algorithm [42]. In essence, it replaces a soundproof density and elliptic pressure (perturbation) with the prognosed thermodynamic density and pressure. Thus it minimises numerical differences between soundproof and compressible algorithms, and provides the reference solution for large-time-step compressible schemes for atmospheric flows. Furthermore, it represents a minimal programming effort to extend the existing soundproof modelling framework to

compressible all-scale flows. Finally, this acoustic scheme forms the foundation of the semi-implicit compressible models with large time steps, discussed next.

3.2.3 Helmholtz solvers for semi-implicit compressible models

A common feature of the anelastic and pseudo-incompressible equations in the generalised system of conservation laws (26)-(28), and thus in (31)-(32), is that the density is prescribed. This obviates the solution of the prognostic mass continuity equation and reduces the first step (40) of the consistent framework to a soundproof predictor (e.g., the linear extrapolation from t^{n-1} and t^n) of $\mathbf{V}^{n+1/2}$ for the use in (37). Furthermore, with the density prescribed (and assuming stationary coordinates), (31) takes a compact form

$$\nabla \cdot (\varrho^* \mathbf{v}) = 0 \ . \tag{48}$$

Because $\mathbf{v} = \widetilde{\mathbf{G}}^T \mathbf{u}$, acting with $\widetilde{\mathbf{G}}^T$ on both sides of (47), multiplying the resulting equation by ϱ^*, acting on it with $\nabla\cdot$, and multiplying the result by $-\delta t/\varrho^*$, produces

$$0 = -\frac{\delta t}{\varrho^*} \nabla \cdot (\varrho^* \mathbf{v}^\nu) = -\frac{\delta t}{\varrho^*} \nabla \cdot \left[\varrho^* \left(\check{\mathbf{v}} - \widetilde{\mathbf{G}}^T \mathbf{C} \nabla \varphi^\nu \right) \right] \ , \tag{49}$$

a (diagonally preconditioned) elliptic Poisson problem for pressure perturbation φ^ν, the solution of which depends on the explicit part

$$\check{\mathbf{v}} = \widetilde{\mathbf{G}}^T \check{\mathbf{u}} \tag{50}$$

and the boundary conditions imposed on the normal component $\mathbf{n}\cdot\mathbf{v}^\nu$ [67,65,41]. In soundproof models, (49) replaces the thermodynamic pressure perturbation of (43), with all other steps of the procedure (41)-(47) remaining the same. Because the soundproof models do not support acoustic modes by design, the stability of the semi-implicit scheme is controlled solely by the advective CFL. The latter is a desirable feature in simulation of low Mach number flows.

Generally, soundproof models are mathematically reduced from the Euler equations to assure that they possess conservation principles, energy invariants in particular, and that their solutions converge asymptotically to respective compressible solutions [35,36,19,20,4,16]. Consequently, their forms, coefficients and reference profiles are theoretically predetermined, providing a strict guidance for the numerical design. In particular, the soundproof form of the mass continuity equation (48) directly implies the associated implicit pressure equation (49). This contrasts with the design of large-time-step semi-implicit schemes for integrating the Euler equations, where the primary guiding principle is the utility of the resulting scheme. Consequently, there is a multitude of numerically-motivated designs of the large-time-step semi-implicit

solvers for the Euler equations, as exemplified by developments in various areas of computational fluid dynamics [22,9,13,38] and computational meteorology [14,6,18,44,77,37,8]. Building on the versatility and robustness of soundproof models, in designing our variants of large-time-step compressible schemes, we recognise that the enhanced stability of soundproof numerics ultimately reduces to constraining the divergence of the flow. A simple numerical experiment can attest to this: proceeding with the semi-implicit acoustic scheme of section 3.2.2, but replacing thermodynamic pressure with the one determined from the incompressibility constraint, produces stable, even if inaccurate results. This suggests that the ultimate cause for acoustic schemes becoming unstable, when violating their sound-speed based CFL, is an uncontrolled growth of truncation errors in determining the pressure gradient force. Consequently, we seek a procedure compensating for such errors while maintaining the consistency between analytic equations and the numerical formulation.

Combining the Cartesian equations (16) and (15) while assuming adiabatic inviscid flows,[8] results in

$$\frac{d\pi}{dt} = -\xi\pi\nabla\cdot\mathbf{u} \implies \frac{\partial\rho\pi}{\partial t} + \nabla\cdot(\rho\pi\mathbf{u}) = -\xi\rho\pi\nabla\cdot\mathbf{u} \tag{51}$$

where $\xi \equiv R_d/c_v$. In the adopted stationary curvilinear framework, (51) takes the form

$$\frac{\partial\varrho^*\pi}{\partial t} + \nabla\cdot(\varrho^*\mathbf{v}\pi) = -\xi\varrho^*\pi\frac{1}{\mathcal{G}}\nabla\cdot(\mathcal{G}\mathbf{v}) \ . \tag{52}$$

This equation is already of the form (32), and we integrate it using a first-order-accurate variant of the NFT template algorithm (37)

$$\pi^{n+1} = \widehat{\pi} - \delta t\xi\pi^{n+1}\frac{1}{\mathcal{G}}\nabla\cdot\left(\mathcal{G}\mathbf{v}^{n+1}\right) + \mathcal{O}(\delta t^2) \ , \tag{53}$$

$$\widehat{\pi} = \mathcal{A}\left(\pi^n, \mathbf{V}^{n+1/2}, \varrho^{*\,n}, \varrho^{*\,n+1}\right)$$

Here, the grid position index $\mathbf{i}$ has been dropped as there is no ambiguity. Except for π^n all remaining arguments of the transport operator are the same as defined in (42). Integrating (52) to the first order still maintains the second-order accuracy of the entire model solution, because pressure perturbations enter the momentum equations with the factor $0.5\delta t$. Multiplying (53) by the constant $c_p\theta_0$, representing π^{n+1} as a sum of the perturbation and the ambient state, expanding $\mathbf{v}^{n+1}$ as a sum of the explicit part of the solution and the pressure gradient force, cf. (49)-(50), and collecting all terms on the rhs, leads

---

[8] Typically, diabatic and viscous effects in weather and climate models enter the governing equations via parameterisations, and simply modify the explicit counterparts of the resulting elliptic problems.

to the elliptic Helmholtz problem

$$0 = -\frac{\delta t}{\mathcal{G}} \nabla \cdot \left[\mathcal{G} \left(\check{\mathbf{v}} - \widetilde{\mathbf{G}}^T \mathbf{C} \nabla \varphi^\nu \right) \right] - \beta(\varphi^\nu - \varphi^\dagger) \ , \tag{54}$$

where $\beta \equiv [\xi(\varphi^{\nu-1} + c_p\theta_0\pi_e)]^{-1}$, $\varphi^\dagger \equiv c_p\theta_0(\widehat{\pi} - \pi_e)$ with $\widehat{\pi}$ denoting the first term on the rhs of (53), and the first guess $\varphi^0 = \varphi^n$ taken for $\varphi^{\nu-1}$. Replacing the explicit thermodynamic pressure perturbations of (43) with (54), while retaining all other elements of the a semi-implicit acoustic scheme the same, leads to a semi-implicit compressible solver stable for large time steps that are comparable to those admitted in the soundproof models. Notably, (54) requires only minor changes to adapt the variational Krylov subspace solver [59,65] designed for the Poisson problem (49).

Numerical experimentation with the global baroclinic instability benchmark revealed that the large-time-step semi-implicit model actually admits time steps only half of the soundproof models. Closer examination of the derived Helmholtz problem (hereafter referred to as "first kind") unveils that advecting the full Exner pressure in (53) adds an explicit term to the vertical velocity update that is proportional to the vertical part of $\mathbf{v}^{n+1/2} \cdot \nabla\pi_e$, itself proportional to $\sim g/\theta_e$, and arguably degrading the stability of the semi-implicit representation of buoyant motions. To mitigate this aspect, and concomitantly to explore the optional avenues, a variant of the Helmholtz problem can be designed (hereafter "second kind") by formulating (51) in the perturbational form, in analogy to the entropy equation (14) that leads to the implicit treatment of buoyancy forces in the soundproof case,

$$\frac{d\pi'}{dt} = -\xi\pi\nabla \cdot \mathbf{u} - \mathbf{u} \cdot \nabla\pi_e \implies \tag{55}$$
$$\frac{\partial\rho\pi'}{\partial t} + \nabla \cdot (\rho\pi'\mathbf{u}) = -\xi\rho\pi\nabla \cdot \mathbf{u} - \rho\mathbf{u} \cdot \nabla\pi_e$$

The resulting form (55) augments (51) with the convective derivative term that is absent in the Poisson solver [59,65]. To facilitate the adaptation of the Poisson solver for the resulting Helmholtz problem of the second kind, we reformulate (55) in a mathematically equivalent conservation form, free of the convective derivative. Rewriting the last term on the rhs of the second equation in (55) as $\rho\mathbf{u} \cdot \nabla\pi_e = \nabla \cdot (\pi_e\rho\mathbf{u}) - \pi_e\nabla \cdot (\rho\mathbf{u})$, expressing the result in the curvilinear coordinates and manipulating terms, we arrive at

$$\frac{\partial\varrho^*\pi'}{\partial t} + \nabla \cdot (\varrho^*\mathbf{v}\pi') = \tag{56}$$
$$-\left[\xi\varrho^*\pi\frac{1}{\mathcal{G}}\nabla \cdot (\mathcal{G}\mathbf{v}) + \nabla \cdot (\varrho^*\mathbf{v}\pi_e) - \pi_e\nabla \cdot (\varrho^*\mathbf{v}) \right] \ ,$$

which after integrating with the NFT scheme similarly to (53) and further manipulating the terms becomes

$$0 = - \delta t \left[\frac{1}{\mathcal{G}} \nabla \cdot (\mathcal{G} \mathbf{v}) + \frac{1}{\xi} \frac{\pi_e}{\pi} \frac{1}{\varrho^* \pi_e} \nabla \cdot (\varrho^* \pi_e \mathbf{v}) - \frac{1}{\xi} \frac{\pi_e}{\pi} \frac{1}{\varrho^*} \nabla \cdot (\varrho^* \mathbf{v}) \right] \qquad (57)$$
$$- \beta(\varphi - \widehat{\varphi}) \, ,$$

where $\widehat{\varphi}$ denotes the action of the transport operator on φ. Recalling that $\mathbf{v} = \check{\mathbf{v}} - \widetilde{\mathbf{G}}^T \mathbf{C} \nabla \varphi$, it can be seen that the operator in the square brackets is composed of three Poisson operators like those in (49) and (54), thereby forming the Helmholtz problem of the second kind.

Notably, the Helmholtz operator in (57) contains three different Laplacians, each entering the problem with different weight. While the first two Laplacians are negative definite and thus carry a promise of converging Krylov schemes, the third Laplacian enters with the opposite sign. However, the second and the third Laplacian combine into a convective derivative of the ambient pressure, resulting in a benign term causing neither growth nor decay of the residual error norms. Diagnosing all terms of the Helmholtz operator (57) in extensive numerical experimentation shows that the total operator is dominated by the first Laplacian and therefore definite.

4 RESULTS

In the following, we discuss results generated with the consistent numerical framework presented in the preceding section, applied to address two distinct classes of atmospheric flows. The first example demonstrates the relative performance of soundproof and compressible models in archetype simulations of planetary weather, whereas the second example addresses mesoscale gravity wave dynamics at nonhydrostatic resolutions. Simulations of both problems using soundproof NFT numerics were already thoroughly documented in the literature [43,64,65]. Here we focus on substantiating the theoretical development of the preceding sections, while providing only brief outlines of the two problems' physical significance and the model setups.

4.1 Global baroclinic instability

In [43], the authors adopted the global baroclinic instability benchmark of [23] for the NFT integrations of the Lipps-Hemler anelastic nonhydrostatic equations (5)-(7). We refer the interested reader to the latter work for the details of implementation, grid convergence study and a thorough discussion of the comparison with the hydrostatic primitive-equation results in [23]. Further results using anelastic and pseudo-incompressible equations with explicit and implicit representation of buoyant modes as well as flux-form Eulerian and semi-

Lagrangian NFT integrators were presented in [64]; the semi-Lagrangian NFT integrators for the consistent framework are highlighted in the appendix C. The analytically prescribed ambient state consists of two mid-latitude zonal jets symmetric about the equator, in (unstable) equilibrium with the corresponding meridional distribution of the potential temperature. The applied initial velocity perturbation localised at the northerly jet excites the development of the instability, with fastest growing, eastward propagating Rossby modes of the (zonal) wavenumber 6. As the instability progresses, the wave steepens and forms sharp overturning fronts (in the horizontal) by day 8, characteristic of natural weather systems at synoptic scales. By the day 10, the northerly jet becomes turbulent. The calculations reported follow the setups of [64], with second-order numerics on a proof-of-concept coarse 64×128 (2.8^o) latitude-longitude grid and 23 km deep atmosphere resolved with 47 uniform δz intervals. The soundproof calculations and the semi-implicit compressible solver of the second kind use 2880 time steps $\delta t = 300$ s, whereas the semi-implicit compressible solver of the first kind uses 5760 of twice-smaller δt. The compressible calculations with explicit representation of acoustic modes employ 432000 times steps $\delta t = 2$ s. The horizontal grid is distributed over the 8×16 processor array of the IBM "Power 7" machine. The resulting wallclock times of the 10 day integrations for the anelastic, pseudo-incompressible, semi-implicit compressible solvers of the first and the second kind, and the acoustic calculations are 2.1, 2.3, 3.7, 2.0, and 178.9 min, respectively. The corresponding wallclock times per time step are: 0.044, 0.048, 0.039, 0.041, and 0.025 s.

Figure 1 complements figure 4 in [64] with the display of instantaneous surface potential temperature perturbations about the ambient equilibrium for the conservative NFT solutions of fully compressible Euler equations, integrated with the semi-implicit large-time-step solvers of the second and the first kind, as well as the acoustic reference algorithm of section 3.2.2. The differences between the three results are insignificant, which is not surprising as the time scale of the global baroclinic instability development (days) is well resolved with both large time steps (300 and 150 s) and acoustic (2 s) δt. To assess the solution correspondence of the compressible and soundproof equations, Fig. 2 displays the large-time step $\delta t = 300$ s results for the compressible, pseudo-incompressible, and anelastic PDEs. Juxtaposing Figs. 1 and 2, reveals that the propagation of baroclinic eddies is the slowest in three compressible runs, faster for the pseudo-incompressible case and the fastest (at about 1 $\mathrm{m\,s}^{-1}$ compared to the compressible solutions) for the anelastic case. While the compressible and pseudo-incompressible solutions agree in amplitude well, the anelastic result (displayed with half of the contour interval) evinces an about twice smaller amplitude of the perturbations and of the maximal wind. The corresponding semi-Lagrangian experiments (not shown) corroborate this relative disparity between the anelastic and the pseudo-incompressible or compressible simulations, even though the amplitude of all semi-Lagrangian results is about 20% smaller than of the corresponding conservative Eulerian results.
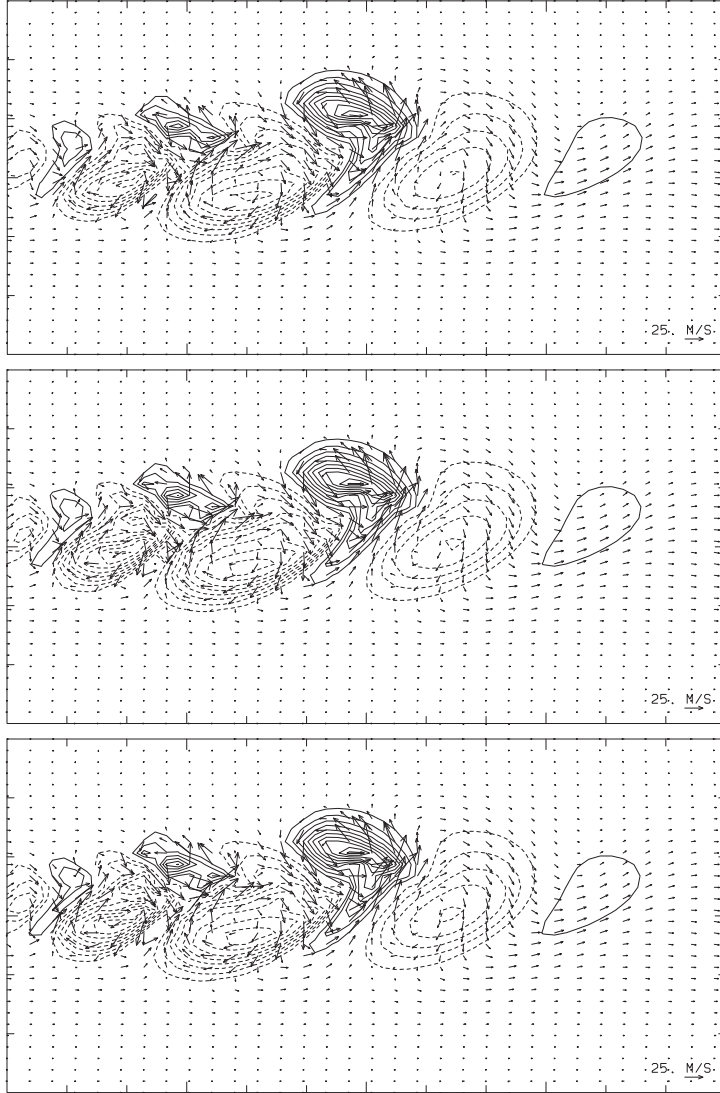
Fig. 1. Baroclinic instability, day 8: surface potential temperature perturbations on the horizontal subdomain $[90, 270] \times [0, 90]$ degrees, for compressible Euler equations integrated with the semi-implicit large-time-step algorithms of the first and second kind (top and centre, respectively) and the acoustic algorithm (bottom). Positive/negative contour values are displayed with solid/dashed lines, and zero contour lines are not shown; the contour interval is 4 K, and the corresponding maximal horizontal wind vectors are 48.5, 47.0 and 44.2 $\mathrm{m\,s^{-1}}$.

Large-time-step calculations at twice finer resolution in each horizontal direction also corroborate this.

The suitability of soundproof models for weather and climate prediction has been questioned on the grounds of normal-mode analysis [17,4]. The present results substantiate the latter, by documenting faster propagation of the soundproof solutions. The results also show that approximating some thermody-
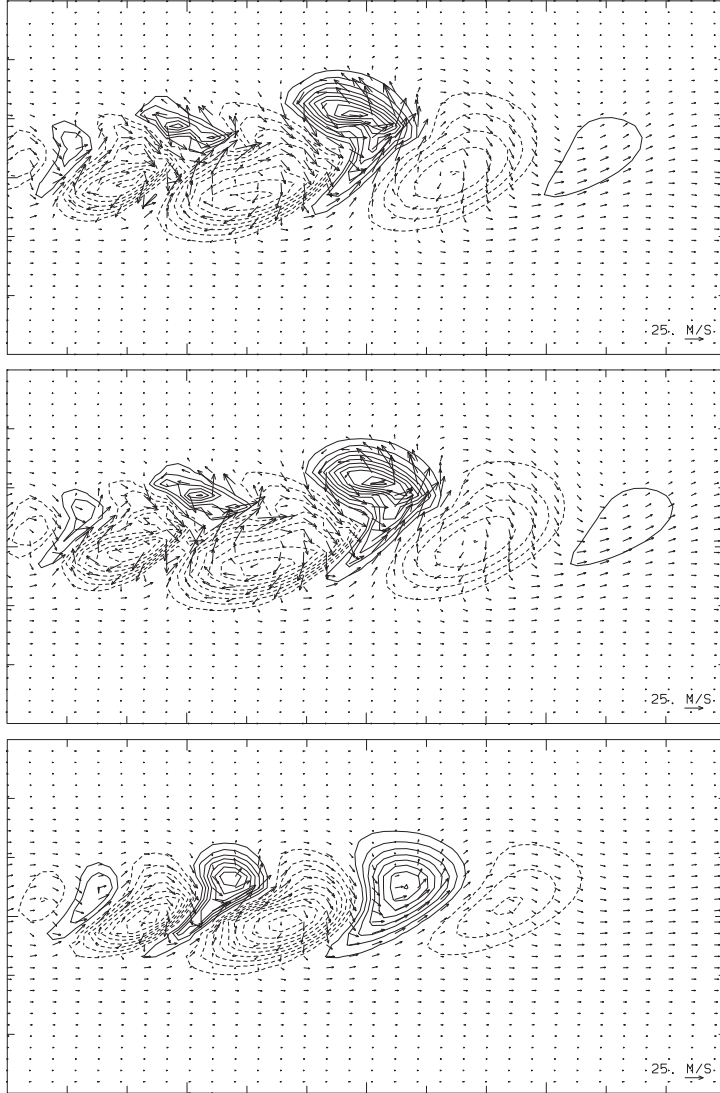
Fig. 2. As Fig. 1, but comparing the $\delta t = 300\ s$ large-time-step solutions for the compressible (top), pseudo-incompressible (centre) and anelastic (bottom) nonhydrostatic models. The contour interval is 2 K for the anelastic run and 4 K otherwise. The respective maximal horizontal wind vectors are 44.2, 49.8, and 28.9 m s^{-1}

namic quantities by reference values cannot be universally accurate. In particular, the comparison of compressible and anelastic solutions emphasises the importance of nonlinear effects; namely the inadequacy of the pressure gradient term linearisation. Figures 2 and 3 show significantly steeper fronts for the pseudo-incompressible and compressible results, while the differences appear relatively insignificant in earlier linear stages of the wave development [43,64]. Figure 3 displays the anelastic, pseudo-incompressible and compressible isentropes in the vertical cross-sections along the meridian passing through the strongest eddy in the centre of the horizontal domain of Figs. 1 and 2. Figure 3
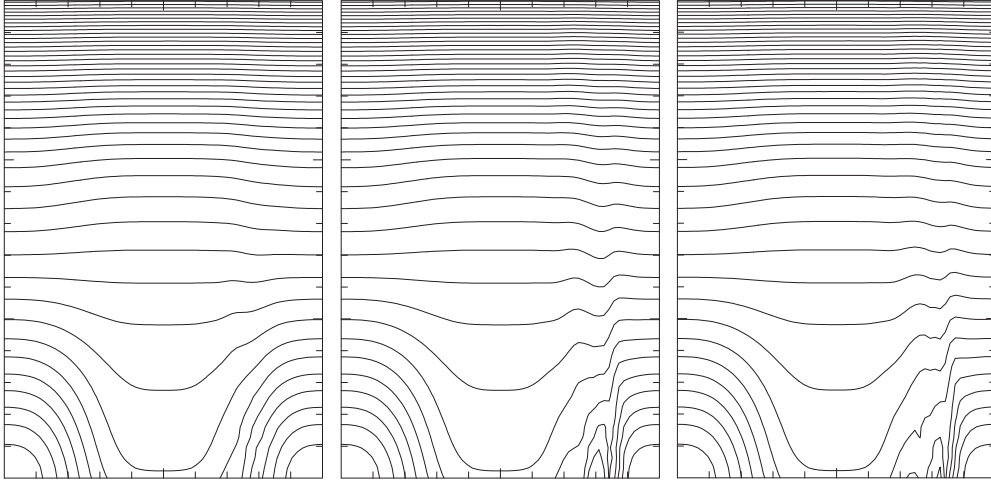
Fig. 3. Isentropes in the vertical cross section along the central meridian of Figs. 1 and 2 for the anelastic (left), pseudo-incompressible (centre) and acoustic compressible (right) models; maximal θ is 736 K at the top of the domain decreasing with contour interval $\approx$ 12 K to 240 K minima at the surface in polar regions.

confirms nearly vertical isentropes in mid-latitudes of the northern hemisphere in the pseudo-incompressible and the compressible result. Furthermore, an ad-hoc numerical experiment with the full θ coefficient imposed arbitrarily in front of the pressure gradient of the anelastic model restores this compressible behaviour. In contrast, replacing the pseudo-incompressible density with the anelastic one has little influence on the pseudo-incompressible result. Similarly, imposing in front of the anelastic pressure gradient either the base state θ_b or the ambient state θ_e, in lieu of full θ, has no substantial effect. The discussed effect is transient, as the anelastic solution also produces steep fronts by day 10 and ultimately all solutions transition to turbulent jets, indistinguishable by day 30 (not shown). While such effects are significant for NWP, due to the transiency they may have a lesser impact on numerical climate prediction, as suggested by the comparability of the anelastic and compressible simulations of the idealised Held-Suarez climate [75] or aquaplanet studies [1,2].

4.2 *Amplification and breaking of stratospheric gravity wave*

The example of the preceding section addressed 3D hydrostatic dynamics even though simulated with nonhydrostatic equations. Here we consider an essentially nonhydrostatic 2D problem. A small amplitude wave packet — excited, say, by a squall line with the top impinging upon the tropopause [40] — propagates into the stratosphere. Because density of the media decreases with altitude, the amplitude of the wave increases with height in proportion to $\rho_b^{-1/2}$. When the wave amplitude becomes comparable with the vertical wave-

length, the problem becomes inherently nonlinear. Then, the wave overturns and breaks generating bursts of turbulence far from the excitation region. The problem is numerically challenging, because it covers about nine density height scales and vertical wavelengths, and a transition from the linear-wave regime near the bottom of the domain to a vigorous turbulent flow with a broad range of scales about 30 km aloft. It has been recently documented in [65], where the soundproof NFT solutions generated on structured grids and unstructured meshes were analysed in the context of asymptotic theory [3].

Following [65], the model setup assumes an isothermal stratosphere, with temperature $T_o = 222.65$ K, and uniform potential temperature stratification $S_\theta = d \ln \theta_b / dz = 4.4 \cdot 10^{-5}$ m^{-1}. The background density decreases exponentially, such that $S_\rho = -d \ln \rho_b / dz = 1.535 \cdot 10^{-4}$ m^{-1}, so the corresponding density scale $H_\rho = 1/S_\rho = 6515$ m is 3.5 times smaller than the potential temperature scale $H_\theta = 1/S_\theta$. The ambient wind $\mathbf{u}_e = (u_e, 0)$ is constant with speed $u_e = U = 20$ m s^{-1}, and the ambient profile of potential temperature $\theta_e(z) = \theta_b$. The 60 km deep and 120 km wide model domain is resolved (in transformed computational domain using terrain-following curvilinear coordinates) with 319×159 uniform grid intervals $\delta x \approx \delta z \approx 380$ m. The wave is excited by a small deflection of the lower boundary with the height profile $h(x) = h_o[1 + (x/L)^2]^{-1}$ centred at the origin of the $[-60L, 60L] \times [0, 60L]$ (x, z)-domain; the deflection's height and half-width are, respectively, $h_o = 628.319$ m and $L = 1000$ m. The problem is inherently nonhydrostatic because $NL/U \approx 1$, or, in other words, the dominant horizontal wavenumber of the problem, $1/L$, equals the asymptotic wavenumber N/U of the induced waves; where $N = \sqrt{gS_\theta}$ denotes the buoyancy frequency. Furthermore, the problem is only weakly nonlinear (the Froude number $Fr = U/Nh_o \approx 1.6$) with respect to linear Boussinesq theory. The onset of wave breaking in the upper half of the model domain is observed after 90 min of the simulated time.

Figure 4 displays the isentropes ($\ln \theta$) at the onset of breaking, simulated with the semi-implicit compressible solver (of the second kind) and the pseudo-incompressible and anelastic soundproof solvers. All large-time-step calculations (including the semi-implicit compressible solver of the 1st kind; not shown) employed the soundproof time step $\delta t = 5$ s. All calculations with soundproof δt were conducted on 32 cores of the IBM "Power 7" machine with insignificant (less than a minute) wall clock time. In agreement with [26,65], the two soundproof systems produce virtually the same solution, also closely matched by the large-time-step semi-implicit compressible solvers, and all break at the same level and at the same time.

Figure 5 shows the equivalent solutions using the acoustic $\delta t = 0.5$ s, 10 times smaller then the soundproof time step used in Fig.4; the actual acoustic solution is not shown, as it closely matches the semi-implicit results in the top panel. The three solutions reproduce the large-time-step solutions at gravity-
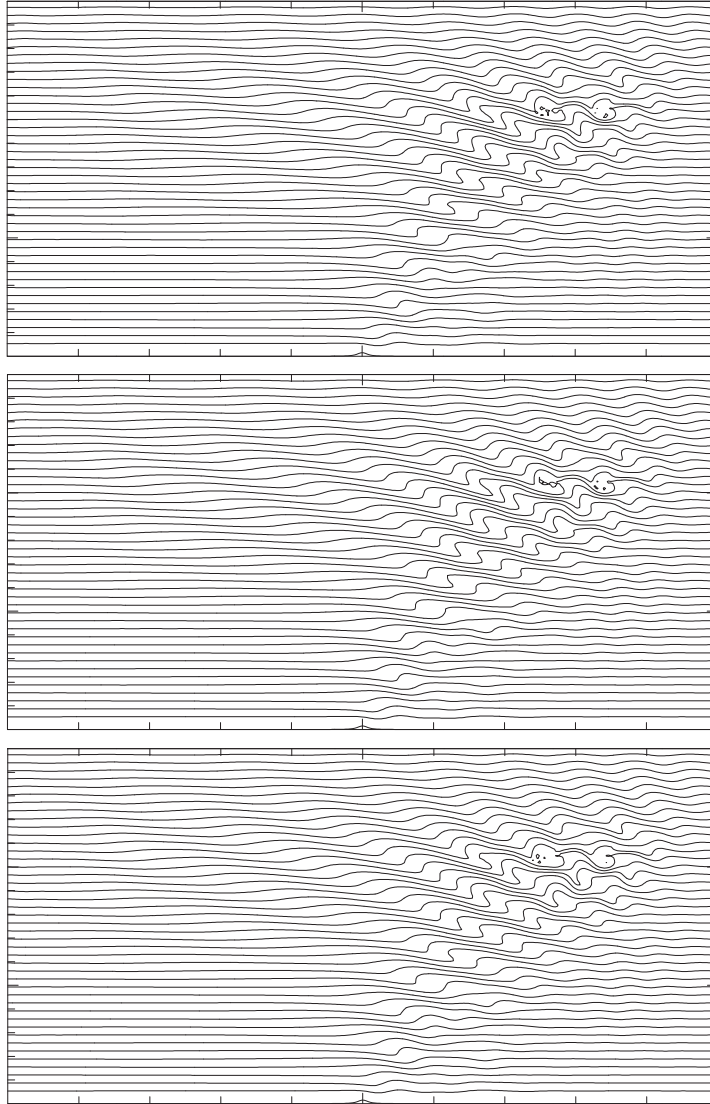
Fig. 4. Isentropes ($\ln\theta$) at the onset of breaking simulated with the semi-implicit compressible solver of the second kind (top), and the pseudo-incompressible and anelastic soundproof solvers (centre and bottom, respectively).

wave scale and closely compare in their fine-scale details. However, they differ in fine scales from the large-time-step solutions in Fig.4, by evincing turbulence more advanced in time; cf. [40] for an extended study of the gravity wave field evolution in a deep atmosphere. Further analysis reveals that all solutions closely match each other in the linear phase (up to 72 min of the simulated time when waves begin to steepen). Afterwards, the acoustic-time-step solutions become visibly more advanced in time (by about 6 min at the 90 min time of Figs. 4 and 5). This contrasts with the baroclinic instability problem, for which all scales of motion remain well resolved in time. Here, at the onset of breaking, the horizontal and vertical velocities roughly dou-
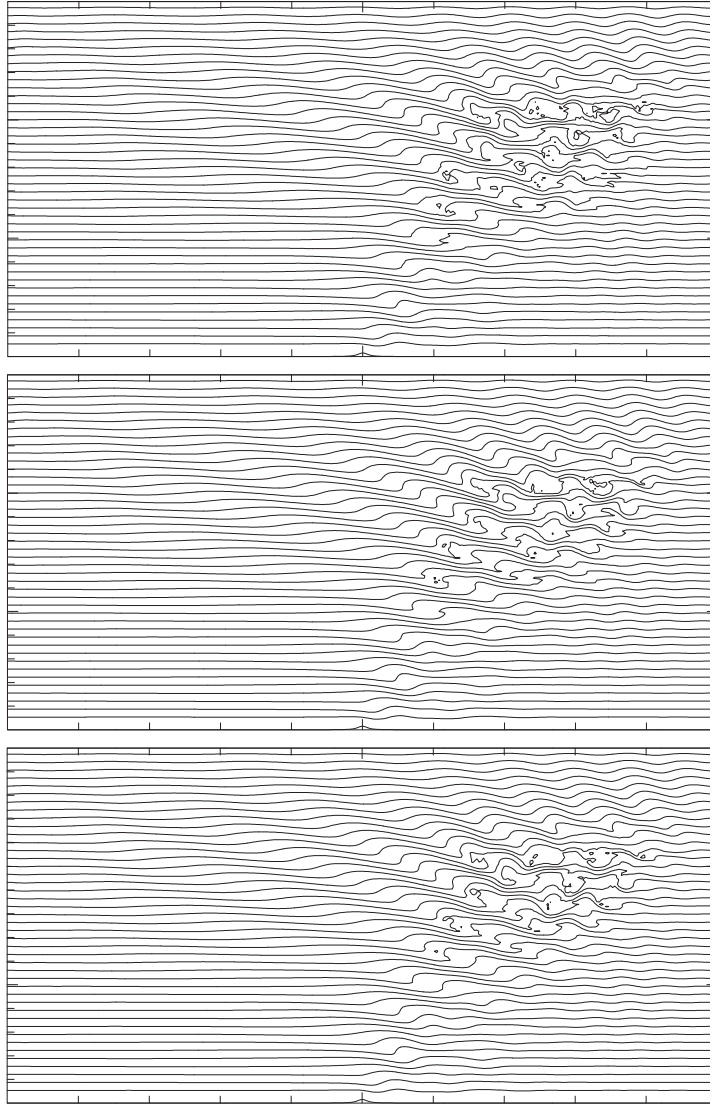
Fig. 5. As in Fig. 4 but for calculations with the acoustic δt.

ble the ambient flow, resulting in Courant numbers 0.8-0.9 for the large δt. With convective motions marginally resolved in time, it is not surprising that the soundproof and acoustic time-step solutions do not match at turbulent scales. Importantly, the comparability of the solutions at either large or small time steps demonstrates the consistent simulation of the soundproof and the compressible equations throughout a range of Courant numbers.

5 REMARKS

In this paper, a class of non-oscillatory forward-in-time (NFT) methods for integrating soundproof equations of atmospheric dynamics [30] has been syn-

thesised with the corresponding NFT solvers for gas dynamics [63], to form a consistent numerical framework for integrating conservation laws of low Mach number, high Reynolds number, rotating stratified flows under gravity underlying all-scale atmospheric dynamics. The foundation of the synthesis lies in assigning the dual, primordial role to the prognostic mass continuity equation: first as a prognostic thermodynamic variable, standard in gas dynamics; and second as a weighting factor shaping conservation laws for specific dependent variables (i.e., expressed per unit of mass), standard in soundproof models. In consequence of the latter, prognosis of the thermodynamic density also defines transportive momenta for subsequent advection of specific variables as cumulative directional mass fluxes. This offers several advantages for the effective prognosis of the specific variables. Given that both density and all specific variables use the same transport algorithm, advection of specific variables preserves their local constancy. Furthermore, flux-limiting of specific variables is consistent with their Lagrangian properties and synchronised naturally with the limiting of the density. Most importantly, even though conservative, the solution is directly specified in terms of specific variables, and this facilitates the design of semi-implicit solvers for compressible systems.

The presented framework stems from the earlier soundproof experience that necessitates an effective solution to generalised Poisson problems like the one in (49), which is elementary to any soundproof system. It turns out that extending proven Krylov solvers to corresponding Helmholtz equations like (54) or (57) is a research topic in itself. In contrast to soundproof models where the elliptic mass-continuity constraints follow the theory of the soundproof equations, constraining flow divergence for the sake of soundproof-time-step integrations of compressible equations has a degree of freedom admitting many forms. The two optional forms of the Helmholtz problem where derived with a view to compensate for truncation errors causing the instability of acoustic schemes at the larger soundproof time steps. The Helmholtz problem (54) is straightforward to derive, reminiscent of similar problems discussed in the literature, and nearly effortless to incorporate into the preexisting Poisson solver for (49). Nonetheless, this led to a semi-implicit compressible model algorithm with impaired stability properties compared to the corresponding soundproof models. In contrast, the Helmholtz problem in (57) proves to be superior and robust, but its derivation and implementation is more involved.

There is another noteworthy aspect, distinguishing implicit compressible solvers from their corresponding soundproof analogues. Solving global soundproof equations in a thin spherical shell of the terrestrial atmosphere, necessarily requires direct matrix inversion in the thin direction, and thus necessitates bespoke preconditioners [59]. In contrast, the semi-implicit compressible solutions in section 4.1, can be obtained with elementary Krylov solvers using no preconditioning, but at substantial expense. On the other hand, employing block-tridiagonal preconditioners in the vertical [59] produces robust and sta-

ble solutions even at the minimal expense of two evaluations of the Helmholtz operator in (57) per solve. Executing the compressible solver with the same stopping criterion as adopted for the soundproof models [66] gives two orders of magnitude smaller norms of the residual error. However, the corresponding results are virtually indistinguishable from the cheaper run with 2 as opposed to 12 evaluations of the Helmholtz operator per solve. This elevates the role of soundproof solvers as building blocks for corresponding, yet computationally more efficient, semi-implicit compressible solvers for atmospheric flows.

In computational meteorology the soundproof and compressible models are often opposed against each other as exclusive schools of thought. Indeed, the results of the current study show substantial differences between the soundproof and compressible solutions at planetary scales that verify and extend theoretical predictions of linear and scale analyses. On the other hand, this study also shows that soundproof and compressible models compose complementary elements of a more general theoretical/numerical approach. In particular, the respective PDEs can be integrated using essentially the same numerics, and this offers new ways for extending soundproof models to fully compressible PDEs. Quite likely, future global atmospheric models will hybridise the strengths of various theoretical formulations (viz. equations), integration schemes and discretisation methods. One idea is to augment the hydrostatic compressible NWP legacy codes with expertise and skills of nonhydrostatic cloud-resolving soundproof research codes [4,29]. A common framework capable of accommodating compressible and soundproof fluid equations with spatial discretisation on structured grids and unstructured meshes [67] is a consequent step towards such a design.

Appendix A. Highlights of MPDATA

The essence of the MPDATA approach is the iterative application of the first-order accurate, sign-preserving generic upwind scheme, with the first iteration providing a first-order-accurate solution, and subsequent iterations compensating for errors of the preceding iterations. Using the notation of section 3.1, the integral (36) of the homogeneous generalised transport equation (33) can be represented [30] as

$$\Psi_{\mathbf{i}} = \mathcal{A}_{\mathbf{i}}\left(\Psi^n, \mathbf{V}^{n+1/2}, G^n, G^{n+1}\right) = \chi_{\mathbf{i}}^{n+1/2} \mathcal{A}_{\mathbf{i}}^o\left(\Psi^n, \boldsymbol{\mathcal{V}}^{n+1/2}, G^n, \chi^{n+1/2}\right) \quad (58)$$
$$= \chi_{\mathbf{i}}^{n+1/2} \, \Psi_{\mathbf{i}}^{(IORD)} \; .$$

where $\chi^{n+1/2} \equiv G^n/G^{n+1}$, and $\mathcal{A}^o$ refers to the established MPDATA scheme, originated in [51,52] for G independent of time and a nonnegative scalar field $\Psi \geq 0$. Specifically, $\mathcal{A}^o$ iterates for $k = 1, IORD$ the discrete flux-form

$$\Psi_{\mathbf{i}}^{(k)} = \Psi_{\mathbf{i}}^{(k-1)} \qquad\qquad\qquad\qquad\qquad\qquad\qquad (59)$$
$$-\frac{1}{G_{\mathbf{i}}}\sum_{I=1}^{N}\left\{ F\left(\Psi_{\mathbf{i}}^{(k-1)}, \Psi_{\mathbf{i+e}_I}^{(k-1)}, \mathcal{V}_{\mathbf{i+1/2e}_I}^{I\,(k)}\right) - F\left(\Psi_{\mathbf{i-e}_I}^{(k-1)}, \Psi_{\mathbf{i}}^{(k-1)}, \mathcal{V}_{\mathbf{i-1/2e}_I}^{I\,(k)}\right)\right\} \; ,$$

where $\mathbf{e}_I$ represents the unit vector in the Ith of the N spatial directions, and integer and half integer indices corresponding to the cell centres and edges of regular computational grid. The superscripts in parentheses number the inner MPDATA iterations, not the time levels. The upwind flux functions F in (59) can be stated in a symbolic form as

$$F\left(\Psi_L, \Psi_R, \mathcal{V}\right) \equiv \max(0, \mathcal{V})\,\Psi_L + \min(0, \mathcal{V})\,\Psi_R \; . \qquad\qquad (60)$$

The algorithm is initialised with $\Psi^{(0)} \equiv \Psi^n$, $\mathcal{V}^{I,(1)} \equiv (\delta t/\delta x^I)(V^I)^{n+1/2}$, where δx^I is spatial grid increments in the Ith coordinate direction. Assumed here is the availability of a $\mathcal{O}(\delta t^2)$ estimate for the generalised local Courant number $\mathcal{V}^I$ at the intermediate time level $t^{n+1/2}$ discussed in the body of the paper. The functional dependence of the error-compensating velocities $(\times \delta t/\delta x^I)$ with $k > 1$ in (59) can be written as

$$\mathcal{V}^{I\,(k)} = \mathcal{V}^I\left(\boldsymbol{\mathcal{V}}^{(k-1)}, \check{\Psi}^{(k-1)}, \nabla\check{\Psi}^{(k-1)}, G^n\right) \; , \quad \check{\Psi} := \chi^{n+1/2}\Psi \; . \qquad (61)$$

The appearance of Ψ in (61) indicates the fundamental nonlinear character of the scheme. The explicit expressions of the error-compensating velocities (61) underlying MPDATA can be found in [51,52,56] for structured grids and in [60,69] for unstructured meshes. For illustration of the basic second-order scheme on structured grids, the symbolic expression (61) encapsulates discrete representations of

$$\mathbf{V}^{k>1} = \frac{1}{2}|\delta\mathbf{x}\cdot\mathbf{V}|\frac{\nabla|\check{\Psi}|}{|\check{\Psi}|} - \frac{1}{2}\delta t G^{-1}\left[\mathbf{V}\left(\mathbf{V}\cdot\frac{\nabla|\check{\Psi}|}{|\check{\Psi}|}\right) + \left(\frac{\partial G}{\partial t} + \nabla\cdot\mathbf{V}\right)\mathbf{V}\right] \quad (62)$$

The concept underlying the MPDATA transport of a nonnegative scalar field can be summarised in a few lines: 1) combine the temporal truncation error as in the second term on the rhs of (35) with the first order spatial discretisation of (60), $\mathcal{O}(\delta\mathbf{x}) = \nabla\cdot(0.5|\delta\mathbf{x}\cdot\mathbf{V}|\nabla\Psi)$; 2) express the cumulative leading error, loosely, as a generalised Laplacian $\nabla\cdot(\mathbf{K}\nabla\Psi)$ with $\mathbf{K}$ symbolising coefficient

matrix; 3) represent the total error as a divergence of the convective flux $\mathcal{O}(\delta t, \delta\mathbf{x}) = -\nabla \cdot (\mathbf{V}_{Err}\Psi)$ with $\mathbf{V}_{Err} = -\mathbf{K}(\Psi^{-1}\nabla\Psi)$; 4) compensate for the error of the preceding upwind iteration by following with another upwind iteration but with an "anti-error velocity" $\mathbf{V}^{k>1} := -\mathbf{V}_{Err}$.

There are numerous options available that extend MPDATA to full monotonicity preservation, third-order accuracy, and variable-sign fields [57,61]; all calculations reported in this paper use the monotone "infinite-gauge" variant of MPDATA, cf. section 5.1 in [60]. MPDATA schemes have numerous advantages, including nonlinear stability, robustness, physical realisability, and massively-parallel scalability [42,39].

Appendix B. Transportive momenta for specific variables in compressible flows: further details

The transportive momenta $\mathbf{V}^{n+1/2} = \overline{(\mathcal{G}\varrho\mathbf{v})}^{n+1/2}$ introduced in section 3.2.1 are technically specified in terms of the generalised local Courant numbers $\mathcal{V}^I$ according to

$$\forall_I \quad \mathcal{V}^{I,(1)}_{\mathbf{i}+1/2\mathbf{e}_I} = \sum_{k=1}^{IORD} F\left(\varrho^{(k-1)}_{\mathbf{i}}, \varrho^{(k-1)}_{\mathbf{i}+\mathbf{e}_I}, \mathbf{e}_I \cdot \boldsymbol{v}^{(k)}_{\mathbf{i}+1/2\mathbf{e}_I}\right) \ , \tag{63}$$

as cumulative donor-cell mass fluxes over the number of MPDATA iterations $IORD$ in the integration of the mass continuity equation (40). In (63),

$$\mathbf{e}_I \cdot \boldsymbol{v}^{(1)} = \frac{\delta t}{\delta x^I}\mathbf{e}_I \cdot \left(\mathcal{G}\mathbf{v}\right)^{n+1/2} \tag{64}$$

is the vector of local Courant numbers composed of transportive velocity $\mathcal{G}\mathbf{v}$ for the advection of density ϱ, whereas for $k > 1$

$$\mathbf{e}_I \cdot \boldsymbol{v}^{(k)} = \mathcal{V}^I\left(\boldsymbol{v}^{(k-1)}, \varrho^{(k-1)}, \nabla\varrho^{(k-1)}, \mathcal{G}\right) \ . \tag{65}$$

according to the functional relation (61) with $\varrho^{(k-1)}$ in lieu of $\Psi^{(k-1)}$.

Appendix C. Semi-Lagrangian congruence

The thrust and attraction of the consistent framework is its conservativity, even though while solving for specific variables governed by the Lagrangian form of the fluid equations. The flux-form NFT schemes have a congruent semi-Lagrangian formulation [54,56,66]. In particular, the template (37) also applies to trapezoidal trajectory integrations of the generalised set of PDEs (17)-(19),

but with the flux-form transport operator $\mathcal{A}$ replaced by the remapping of transported fields of specific variables to departure points of the trajectories $\mathbf{x}_o\big((\mathbf{x_i}, t^{n+1}), t^n\big)$ at t^n that arrive at the grid points $\mathbf{x_i}$ at t^{n+1}. The remapping itself equally uses NFT advection schemes akin to MPDATA [54,55]. In the semi-Lagrangian option, the evaluation of transportive momenta is replaced with calculation of the departure point of the trajectories, so that step (40) is obviated, whereas the compressible mass continuity equation (15) is integrated with a second-order Runge-Kutta scheme

$$\varrho_{\mathbf{i}}^{n+1} = \widehat{\varrho}_{\mathbf{i}} - 0.5\delta t \left(\frac{\varrho}{\mathcal{G}} \nabla \cdot (\mathcal{G}\check{\mathbf{v}}) \right)_{\mathbf{i}}^{n+1} . \tag{66}$$

Here, $\widehat{\varrho}_{\mathbf{i}} = [\varrho(1 - 0.5\delta t \mathcal{G}^{-1}\nabla \cdot (\mathcal{G}\mathbf{v}))]_o \equiv \widetilde{\varrho}_o$ is a field of values remapped to the departure points of the trajectories, and $\check{\mathbf{v}}$ is a $\mathcal{O}(\delta t^2)$ estimate of $\mathbf{v}$. In this notation, the closed form of (66) becomes

$$\varrho_{\mathbf{i}}^{n+1} = \widehat{\varrho}_{\mathbf{i}}/(1 + 0.5\delta t \mathcal{G}^{-1}\nabla \cdot (\mathcal{G}\check{\mathbf{v}}))_{\mathbf{i}}^{n+1} , \tag{67}$$

while the remaining integration proceeds analogously to the semi-implicit scheme, either using the acoustic or large-time-step model algorithm, but with all flux-form transport operations replaced by the remapping to the feet of trajectories.

References

[1] B.J. Abiodun, J.M. Prusa, W.J. Gutowski, Implementation of a non-hydrostatic, adaptive-grid dynamics core in CAM3. Part I: comparison of dynamics cores in aqua-planet simulations, Clim. Dyn. 31 (2008) 795–810.

[2] B.J. Abiodun, W.J. Gutowski, J.M. Prusa, Implementation of a non-hydrostatic, adaptive-grid dynamics core in CAM3. Part II: dynamical influences on ITCZ behavior and tropical precipitation, Clim. Dyn. 31 (2008) 811–822.

[3] U. Achatz, R. Klein, F. Senf (2010), Gravity waves, scale asymptotics and the pseudo-incompressible equations, J. Fluid Mech. 663 (2010) 120–147.

[4] A. Arakawa, C. Konor, Unification of the anelastic and quasi-hydrostatic systems of equations, Month. Weather Rev. 137 (2009), 710–726.

[5] M. Baldauf, A. Seifert, J. Förstner, D. Majewski, M. Raschendorfer, Operational convective-scale numerical weather prediction with the COSMO model: Description and sensitivities, Month. Weather Rev. 139 (2011), 3887–3905.

[6] P. Bénard, Stability of semi-implicit and iterative centered-implicit time discretisation for various equation systems used in NWP, Month. Weather Rev. 131 (2003) 2479–2491.

[7] P. Bénard, J. Vivoda, J. Mašek, P. Smoliková, K. Yessad, Ch. Smith, R. Brožkovaá, J.F. Geleyn, Dynamical kernel of the ALADIN — NH spectral limited-area model: Revised formulation and sensitivity experiments, Q.J.R. Meteorol. Soc. 136 (2010) 155–169.

[8] T. Benacchio, W.P. O'Neill, R. Klein, A blended sound-proof-to-compressible numerical model for atmospheric dynamics, Month. Weather Rev. (2013) submitted.

[9] H. Bijl, P. Wesseling, A unified method for computing incompressible and compressible flows in boundary-fitted coordinates, J. Comput. Phys. 141 (1998) 153–173.

[10] P.N. Blossey, D.R. Durran, Selective monotonicity preservation in scalar advection, J. Comput. Phys. 227 (2008) 5160–5183.

[11] T.L. Clark, Small-scale dynamic-model using a terrain-following coordinate transformation, J. Comput. Phys. 24 (1977) 186–215.

[12] T.L. Clark, R.D. Farley, Severe downslope windstorm calculations in two and three spatial dimensions using anelastic interactive grid nesting: a possible mechanism for gustiness, J. Atmos. Sci. 41 (1984) 329–350.

[13] P. Colella, K. Pao, A projection method for low speed flows, J. Comput. Phys. 149 (1999) 245–269.

[14] M.J.P. Cullen, A test of a semi-implicit integration technique for a fully compressible non-hydrostatic model, Q.J.R. Meteorol. Soc. 116 (1990) 1253–1258.

[15] F.X. Giraldo, J.F. Kelly, E.M. Constantinescu, Implicit-explicit formulations of a three-dimensional nonhydrostatic unified model of the atmosphere (NUMA), SIAM J. Sci. Comput. 35 (2013) B1162–B1194.

[16] C.J. Cotter, D.D. Holm, Variational formulations of sound-proof models, Q.J.R. Meteorol. Soc. (2013) DOI: 10.1002/qj.2260, in press.

[17] T. Davies, A. Staniforth, N. Wood, J. Thuburn, Validity of anelastic and other equation sets as inferred from normal-mode analysis. Q.J.R. Meteorol. Soc. 129 (2003) 2761–2775.

[18] T. Davies, M.J.P. Cullen, A.J. Malcolm, M.H. Mawson, A. Staniforth, A.A White, N. Wood, A new dynamical core for the Met Office's global and regional modelling of the atmosphere. Q.J.R. Meteorol. Soc. 131 (2005) 1759–1782.

[19] D.R. Durran, Improving the anelastic approximation. J. Atmos. Sci. 46 (1989) 1453–1461.

[20] D.R. Durran, A physically motivated approach for filtering acoustic waves from the equations governing compressible stratified flow, J. Fluid Mech. 601 (2008) 365–379.

[21] M. Ghizaru, P. Charbonneau, P.K. Smolarkiewicz, Magnetic Cycles in Global Large-eddy Simulations of Solar Convection, Astrophys. J. Lett. 715 (2010) L133–L137

[22] R.I. Issa, Solution of the implicitly discretised fluid flow equations by operator-splitting, J. Comput. Phys. 62 (1985) 40-65.

[23] C. Jablonowski, D.L. Williamson, A baroclinic instability test case for atmospheric model dynamical cores, Q.J.R. Meteorol. Soc. 132 (2006) 2943–2975.

[24] J.B. Klemp, R.B. Wilhelmson, The simulation of three-dimensional convective storm dynamics, J. Atmos. Sci. 35 (1978) 1070–1096.

[25] R. Klein, Semi-implicit extension of a Godunov-type scheme based on low Mach number asymptotics I: One-dimensional flow, J. Comput. Phys. 121 (1995) 213-237.

[26] R. Klein, Asymptotics, structure, and integration of sound-proof atmospheric flow equations, Theor. Comput. Fluid Dyn. 23 (2009) 161–195.

[27] R. Klein, U. Achatz, D. Bresch, O.M. Knio, P.K. Smolarkiewicz, Regime of validity of soundproof atmospheric flow models, J. Atmos. Sci. 67 (2010) 3226–3237.

[28] R. Klein, On the regime of validity of sound-proof model equations for atmospheric flows. *Proceedings of the ECMWF Workshop on Nonhydrostatic Modelling, 8-10 November, 2010, Reading, UK*, (2011) 35–53.

[29] C. Konor, Design of a Dynamical Core Based on the Nonhydrostatic "Unified System" of Equations. Month. Weather Rev. doi:10.1175/MWR-D-13-00187.1, in press.

[30] C. Kühnlein, P.K. Smolarkiewicz, A. Dörnbrack, Modelling atmospheric flows with adaptive moving meshes, J. Comput. Phys. 231 (2012) 2741–2763.

[31] M. Kurowski, W.W. Grabowski, and P.K. Smolarkiewicz, 2013: Towards multiscale simulation of moist flows with soundproof equations, J. Atmos. Sci. 70 (2013) 3995–4011.

[32] R. Laprise, The Euler equations of motion with hydrostatic pressure as an independent variable, Mon. Weather. Rev. 120 (1992) 197–207.

[33] B. Larrouturou, How to preserve the mass fractions positivity when computing compressible multi-component flows, J. Comput. Phys. 95 (1991) 59-84.

[34] R. Laprise, Regional climate modelling, J. Comput. Phys. 277 (2008) 3641–3666.

[35] F.B. Lipps, R.S. Hemler, A scale analysis of deep moist convection and some related numerical calculations, J. Atmos. Sci. 39 (1982) 2192–2210.

[36] F.B. Lipps, On the anelastic approximation for deep convection, J. Atmos. Sci. 47 (1990) 1794–1798.

[37] E.H. Müller, R. Scheichl, Massively parallel solvers for elliptic PDEs in numerical weather- and climate prediction, Q.J.R. Meteorol. Soc. (2013) submitted.

[38] C.D. Munz, S. Roller, R. Klein, K.J. Geratz, The extension of incompressible flow solvers to the weakly compressible regime, Comput. Fluids 37 (2008) 1193-1207.

[39] Z.P. Piotrowski, A.A. Wyszogrodzki, P.K. Smolarkiewicz, Towards petascale simulations of atmospheric circulations with soundproof models, Acta Geophysica 59 (2011) 1294–1311.

[40] J.M. Prusa, P.K. Smolarkiewicz, R.R. Garcia, Propagation and breaking at high altitudes of gravity waves excited by tropospheric forcing, J. Atmos. Sci. 53 (1996) 2186–2216.

[41] J.M. Prusa, P.K. Smolarkiewicz, An all-scale anelastic model for geophysical flows: dynamic grid deformation, J. Comput. Phys. 190 (2003) 601–622.

[42] J.M. Prusa, P.K. Smolarkiewicz, A.A Wyszogrodzki, EULAG, a computational model for multiscale flows, Comput. Fluids 37 (2008) 1193-1207

[43] J.M. Prusa, W.J. Gutowski, Multi-scale features of baroclinic waves in soundproof, global simulations with EULAG, Proc. V European Conference on Computational Fluid Dynamics, Lisbon, Portugal, 2010, ECCOMAS paper #1453, 18 pp.

[44] J.M. Reisner, V.A. Mousseau, A.A. Wyszogrodzki, D.A. Knoll, An implicitly balanced hurricane model with physics-based preconditioning, Month. Weather Rev. 133 (2005) 1003–1002.

[45] M. Satoh, T. Matsuno, H. Tomita, H. Miura, T. Nasuno, S. Iga, Nonhydrostatic icosahedral atmospheric model (NICAM) for global cloud resolving simulations, J. Comput. Phys. 227 (2008) 3486–3514.

[46] C. Schär, P.K. Smolarkiewicz, A synchronous and iterative flux-correction formalism for coupled transport equations, J. Comput. Phys. 128 (1996) 101–120.

[47] T. Schneider, N. Botta, K.J. Geratz, R. Klein, Extension of finite volume compressible flow solvers to multi-dimensional, variable density zero Mach number flows, J. Comput. Phys., 155 (1999) 248-286.

[48] Y. Seity, P. Brousseau, S. Malardel, G. Hello, P. Bénard, F. Bouttier, C. Lac, V Masson, The AROME-France convective-scale operational model, Month. Weather Rev. 139 (2011) 976–991.

[49] W.C. Skamarock, J.B. Klemp, A time-split nonhydrostatic atmospheric model for weather research and forecasting applications, J. Comput. Phys. 227 (2008) 3465–3485.

[50] W.C. Skamarock, J.B. Klemp, M.G. Duda, L.D. Fowler, S.-H. Park, T.D. Ringler, A multiscale nonhydrostatic atmospheric model using centroidal Voronoi tesselations and C-grid staggering, Month. Weather Rev. 140 (2012) 3090–3105.

[51] P.K. Smolarkiewicz, A fully multidimensional positive definite advection transport algorithm with small implicit diffusion, J. Comput. Phys., 54 (1984) 325–362.

[52] P.K. Smolarkiewicz, T.L. Clark, The multidimensional positive definite advection transport algorithm; Further developments and applications, J. Comput. Phys., 67 (1986) 396–438.

[53] P.K. Smolarkiewicz, W.W. Grabowski, The multidimensional positive definite advection transport algorithm: Nonoscillatory Option, J. Comput. Phys., 86 (1990) 355–375.

[54] P.K. Smolarkiewicz, J.A. Pudykiewicz, A class of semi-Lagrangian approximations for fluids. J. Atmos. Sci. 49 (1992) 2082–2096.

[55] P.K. Smolarkiewicz, G.A. Grell, A class of monotone interpolation schemes, J. Comput. Phys. 101 (1992) 431–440.

[56] P.K. Smolarkiewicz, L.G. Margolin, On forward-in-time differencing for fluids: Extension to a curvilinear framework, Month. Weather Rev. 121 (1993) 1847–1859.

[57] P.K. Smolarkiewicz, L.G. Margolin, MPDATA: A finite-difference solver for geophysical flows, J. Comput. Phys. 140 (1998) 459–480.

[58] P.K. Smolarkiewicz, L.G. Margolin, A.A Wyszogrodzki, A class of nonhydrostatic global models, J. Atmos. Sci. 58 (2001) 349–364.

[59] P.K. Smolarkiewicz, C. Temperton, S.J. Thomas, A.A. Wyszogrodzki, Spectral preconditioners for nonhydrostatic atmospheric models: extreme applications. In: Proc. ECMWF Seminar Series on Recent Developments in Numerical Methods for Atmospheric and Ocean Modelling, 6-10 September, 2004, Reading, UK, 203–220.

[60] P.K. Smolarkiewicz, J. Szmelter, MPDATA: An edge-based unstructured-grid formulation, J. Comput. Phys. 206 (2005) 624–649.

[61] P.K. Smolarkiewicz, Multidimensional positive definite advection transport algorithm: an overview, Int. J. Numer. Meth. Fluids 50 (2006) 1123–1144.

[62] P.K. Smolarkiewicz, A. Dörnbrack, Conservative integrals of adiabatic Durran's equations. Int. J. Numer. Meth. Fluids 56 (2008) 1529–1534.

[63] P.K. Smolarkiewicz, J. Szmelter, Iterated upwind schemes for gas dynamics, J. Comput. Phys. 228 (2009) 33–54.

[64] P.K. Smolarkiewicz, Modeling atmospheric circulations with soundproof equations. *Proceedings of the ECMWF Workshop on Nonhydrostatic Modelling, 8-10 November, 2010, Reading, UK*, (2011) 1–15.

[65] P.K. Smolarkiewicz, J. Szmelter, A nonhydrostatic unstructured-mesh soundproof model for simulation of internal gravity waves, Acta Geophysica 59 (2011) 1109–1134.

[66] P.K. Smolarkiewicz, P. Charbonneau, EULAG, a computational model for multiscale flows: An MHD extension, J. Comput. Phys. 236 (2013) 608–623.

[67] P.K. Smolarkiewicz, J. Szmelter, A.A. Wyszogrodzki, An unstructured-mesh atmospheric model for nonhydrostatic dynamics, J. Comput. Phys. 254 (2013) 184–199.

[68] J. Steppeler, R. Hess, U. Schättler, L. Bonaventura, Review of numerical methods for nonhydrostatic weather prediction models, Meteorol. Atmos. Phys. 82 (2003) 287–301.

[69] J. Szmelter, P.K. Smolarkiewicz, MPDATA error estimator for mesh adaptivity. Int. J. Numer. Meth. Fluids 50 (2006) 1269–1293.

[70] J. Szmelter, P.K. Smolarkiewicz, An edge-based unstructured mesh discretisation in geospherical framework, J. Comput. Phys. 229 (2010) 4980–4995.

[71] M.C. Tapp, P.W. White, A non-hydrostatic mesoscale model. Q.J.R. Meteorol. Soc. 102 (1976) 277–296.

[72] A. Warn-Varnas, J. Hawkins, P.K. Smolarkiewicz, S.A. Chin-Bing, D. King, Z. Hallock, Solitary wave effects north of Strait of Messina, Ocean Modelling 18 (2007) 97–121.

[73] N.P. Wedi, P.K. Smolarkiewicz, Extending Gal-Chen and Somerville terrain-following coordinate transformation on time dependent curvilinear boundaries, J. Comput. Phys. 193 (2004) 1–20.

[74] N.P. Wedi, P.K. Smolarkiewicz, Direct numerical simulation of the Plumb-McEwan laboratory analog of the QBO, J. Atmos. Sci. 63 (2006) 3326–3252.

[75] N.P. Wedi, P.K. Smolarkiewicz, A Framework for testing global nonhydrostatic models, Q.J. Roy. Meteorol. Soc., 135 (2009) 469–484.

[76] N.P. Wedi, M. Hamrud, G. Mozdzynski, G. Austad, S. Curic, J. Bidlot, Global, non-hydrostatic, convection-permitting, medium-range forecasts: progress and challenges. *ECMWF Newsletter No. 133* (2012) 17–22.

[77] N. Wood, A. Staniforth, A. White, T. Allen, M. Diamantakis, M. Gross, T. Melvin, C. Smith, S. Vosper, M. Zerroukat, J. Thuburn, An inherently mass-conserving semi-implicit semi-Lagrangian discretisation of the deep-atmosphere global non-hydrostatic equations, Q.J.R. Meteorol. Soc. DOI: 10.1002/qj.2235, in press.

[78] K.-S. Yeh, J. Côté, S. Gravel, A. Méthot, A. Patoine, M. Roch, A. Staniforth, The CMC-MRB global environmental multiscale (GEM) model. Part III: Nonhydrostatic formulation, Month. Weather Rev. 130 (2002) 339–356.